INTERNATIONAL JOURNAL FOR NUMERICAL METHODS IN ENGINEERING
Int. J. Numer. Meth. Engng 2011; **x**:1–21 *Prepared using* nmeauth.cls *[Version: 2002/09/18 v2.02]*

Direct computation of critical equilibrium states for spatial beams and frames *

Jari Mäkinen[1], Reijo Kouhia[2*], Alexis Fedoroff[2], and Heikki Marjamäki[1]

[1] *Department of Mechanics and Design, Tampere University of Technology, P.O. Box 589, FI-33101 Tampere, Finland*
[2] *Department of Civil and Structural Engineering, Aalto University School of Engineering, P.O. Box 12100, FI-00076 Aalto, Finland*

SUMMARY

In this paper explicit formulas for second order derivatives of the residual vector with respect to the state variables for a geometrically exact 3-D beam element based on the Reissner's model are presented. These derivatives are required when a direct non-linear stability eigenvalue problem is solved by the Newton's method. If the external load is parametrized by a single parameter such an eigenvalue problem consist of solving the critical state variables, the eigenmode and the critical load parameter from the equation system consisting of the equilibrium equations, the criticality condition and some auxiliary conditions depending on the type of a critical point.

KEY WORDS: critical points, equilibrium equations, Newton's method, geometrically exact kinematics, Reissner's beam model, rotation manifold

1. INTRODUCTION

An essential task in computational structural analysis is the determination of the critical loads. If the pre-buckling displacements are small, it is usually sufficient to solve the linearized eigenvalue problem, where the linearization is performed with respect to the undeformed configuration. However, in many cases the pre-buckling deflections have considerable effect on the buckling behaviour and cannot be neglected. Using higher order polynomial eigenvalue formulations, which take the finite pre-buckling deflections into account, is an appealing approach [1, 2, 3, 4, 5]. However, such approaches have not been widely used.

One way to compute the critical points is to use a path-following method to solve the non-linear equilibrium equations and as a byproduct detect the change in stability properties along the traced path. Such an an indirect method is considered e.g. in [6, 7, 8, 9].

*This is a preprint of an article accepted for publication in *IJNME*. Copyright©2011 John Wiley & Sons, Ltd.
*Correspondence to: R. Kouhia, Department of Civil and Structural Engineering, Aalto University School of Engineering, P.O. Box 12100, FI-00076 Aalto, Finland, e-mail: reijo.kouhia@aalto.fi

Received
Revised

A direct method to compute the critical point is so constituted that the equilibrium equations are augmented with a criticality condition. The criticality condition has in some sense to state the vanishing stiffness of the stucture and can be either a scalar equation [10, 11, 12] or an eigenvalue problem [13, 14, 15, 16, 17, 18, 19]. Extension of the direct approach to compute secondary bifurcations is due to Wu [20].

The idea of augmenting the equilibrium equations with the criticality condition appears to be due to Keener and Keller [13], presented as early as in 1973. Most papers found in literature deal only with simple critical points, and the extension to multiple bifurcations, see Keener [21], will not be considered in this paper.

Direct solution of the non-linear stability eigenvalue problem should not be considered as a distinctive alternative to the indirect method. Success of the direct procedure depends heavily on the nearness of the critical point to the initial state.

During the last decades considerable interest towards the development of the geometrically exact formulation for spatial beams, which is not a trivial task, has been payed by several researchers [22, 23, 24, 25, 26, 27, 28, 29, 30, 31, 32]. Geometrically exact model is mandatory for the direct solution of the critical points along the equilibrium path, since it requires complete kinematic description of the underlying mechanical model. In particular, for dimensionally reduced models, like beam- and shell models, the description has to be capable to handle large rotations.

The beam model is called geometrically exact if no other kinematic simplifications during derivation are applied than the basic kinematic hypothesis, like the Timoshenko-Reissner beam hypothesis. In the Timoshenko-Reissner beam hypothesis, transversal shears are allowed, such that a cross-section remains in-plane and one's shape in a deformed state, but the normal of a cross-section is not necessarily parallel with the tangent of the central line. The rotation of the cross-section plane is described by the total rotation vector. Well-known singularity problems are passed by the complement rotation vector that is another parametrization of rotation manifold. The tangential transformation operator of rotation and its derivatives are needed for non-linear analysis of beam models that are well known. However, the direct solution of the critical points for a geometrically exact Reissner's beam model requires some new derivatives of the tangential transformation operator which are given explicitly in this paper.

In this paper procedures for direct computation of critical equilibrium states for spatial beam structures are described. Linearization of the extended system requires second order derivatives of the residual vector with respect to the state variables. For models with rotational degrees of freedom, to the authors knowledge, these derivatives has not been presented before. In this paper the second order derivatives are applied for the geometrically exact Reissner's beam model in deriving the Jacobian matrix of the extended system. However, it should be mentioned that these derivatives are applicable also to other models involving rotational state variables, like shells and polar continuum models. Another novelty is the introduction of a constraint equation which quarantees convergence to a critical point with positive load parameter value.

The outline of the paper is the following. In the next section a brief summary of the procedures for the non-linear eigenvalue problem is given. Both the direct solution and and polynomial approximations are presented. In the third section the geometrically exact beam model is described and the extra matrices required in the non-linear eigenvalue solution procedure are presented. In the section 4 some numerical examples are shown.

2. DETERMINATION OF CRITICAL POINTS

2.1. Non-linear eigenvalue problem

A critical point along an equilibrium path can be determined by solving the non-linear eigenvalue problem: find the critical value of the N-dimensional displacement vector $\mathbf{q}$, the load parameter λ and the corresponding eigenvector $\boldsymbol{\phi}$ such that

$$\left\{ \begin{array}{rcl} \mathbf{f}(\mathbf{q},\lambda) & = & \mathbf{0} \\ \mathbf{f}'(\mathbf{q},\lambda)\boldsymbol{\phi} & = & \mathbf{0} \end{array} \right. \tag{1}$$

where $\mathbf{f}$ is the vector of unbalanced forces and $\mathbf{f}'$ denotes the Gateaux derivative (Jacobian matrix) with respect to the state variables $\mathbf{q}$. Equation $(1)_1$ is the equilibrium equation, which has to be satisfied at the critical point, and equation $(1)_2$ states the zero stiffness in the direction of the critical eigenmode $\boldsymbol{\phi}$, which is the actual criticality condition. Such a system is considered in Refs. [14, 33, 17]. Abbot [10] considers a different extended system where the criticality is identified by means of the determinant of the tangent stiffness matrix. The drawback of this procedure is that the directional derivative of the determinant is difficult to compute. A more recent application of this strategy is due to Planinc and Saje [11]. Battini et al. [12] used the lowest eigenvalue as a criticality indicator and the eigenvalue and eigenmode is updated in a staggered fashion together with the equilibrium equations.

The equilibrium equation $(1)_1$ constitutes the balance of internal forces $\mathbf{r}$ and external loads $\mathbf{p}$, which is usually parametrized by a single variable λ, the load parameter, defining the intensity of the load vector:

$$\mathbf{f}(\mathbf{q},\lambda) := \mathbf{r}(\mathbf{q}) - \lambda \mathbf{p}_{\mathrm{r}}(\mathbf{q}). \tag{2}$$

If the loads does not dependent on deformations, like in dead-weight loading, the reference load vector $\mathbf{p}_{\mathrm{r}}$ is independent of the displacement field $\mathbf{q}$.

The system (1) consists of $2N+1$ unknowns, the displacement vector $\mathbf{q}$, the eigenmode $\boldsymbol{\phi}$ and the load parameter value λ at the critical state. Since the eigenvector $\boldsymbol{\phi}$ is defined uniquely up to a constant, the normalizing condition can be added to the system (1):

$$\mathbf{g}(\mathbf{q},\boldsymbol{\phi},\lambda) = \left\{ \begin{array}{c} \mathbf{f}(\mathbf{q},\lambda) \\ \mathbf{f}'(\mathbf{q},\lambda)\boldsymbol{\phi} \\ c(\boldsymbol{\phi},\lambda) \end{array} \right\} = \mathbf{0}, \tag{3}$$

where the Jacobian matrix $\mathbf{f}' = \partial \mathbf{f}/\partial \mathbf{q}$ is usually denoted by $\mathbf{K}$ in structural applications, and $c(\boldsymbol{\phi})$ defines some normalizing condition to the eigenvector. The Jacobian matrix of the extended system (3) has the form

$$\mathbf{J} = \left[\begin{array}{ccc} \mathbf{K} & \mathbf{0} & -\mathbf{p}_r \\ \mathbf{Z} & \mathbf{K} & \mathbf{n} \\ \mathbf{0}^{\mathrm{T}} & \mathbf{c}_\phi^{\mathrm{T}} & c_\lambda \end{array} \right], \tag{4}$$

where

$$\mathbf{Z} = \left[\mathbf{f}'\boldsymbol{\phi}\right]', \quad \mathbf{n} = \partial(\mathbf{f}'\boldsymbol{\phi})/\partial\lambda, \quad \mathbf{c}_\phi^{\mathrm{T}} = \partial c/\partial\boldsymbol{\phi}, \quad \text{and } c_\lambda = \partial c/\partial\lambda. \tag{5}$$

One problem in using Newton's method to the system (3) is the computation of the matrix $\mathbf{Z}$ and the vector $\mathbf{n}$. Finite difference approximations are usually used in the literature [34, 35, 12, 36, 37, 38, 17].

To quarantee asymptotically quadratic convergence for the Newton's iteration, the Jacobian should be non-singular at the solution point. For Jacobian of the form (4) this is true only for limit points, and the use of system (3) is not necessarily efficient for the computation of bifurcation points [33]. However, it has been used also to compute bifurcation points in Refs. [14, 16]. Also the results in this paper show that the iterations can stay in the quadratic convergence cone in the case of a bifurcation point.

To guarantee the regularity of the Jacobian of the extended system (3), Wriggers and Simo [17] regularized it with penalty terms by appending the constraint $\mathbf{e}_i^T\mathbf{q} = \mu$ to it

$$\mathbf{g}(\mathbf{q},\phi,\lambda,\mu) = \left\{ \begin{array}{c} \mathbf{f}(\mathbf{q},\lambda) + \gamma(\mathbf{e}_i^{\mathrm{T}}\mathbf{q} - \mu)\mathbf{e}_i \\ \mathbf{f}'(\mathbf{q},\lambda)\boldsymbol{\phi} + \gamma(\mathbf{e}_i^{\mathrm{T}}\boldsymbol{\phi} - \phi_0)\mathbf{e}_i \\ \mathbf{e}_i^{\mathrm{T}}\boldsymbol{\phi} - \phi_0 \\ \mathbf{e}_i^{\mathrm{T}}\mathbf{q} - \mu \end{array} \right\} = \mathbf{0}, \tag{6}$$

where γ is a non-negative regularizing penalty parameter and $\mathbf{e}_i$ is a unit vector having the unit value at position i corresponding to the smallest diagonal entry of the factorized tangent stiffness matrix. If the Jacobian of the system (6) is consistently computed, and the initial guess belongs to the domain of attaction, then the Newton's method is quaranteed to converge with asymptotically quadratic rate [39, 40, 41]. However, numerical computations in many cases seem to show asymptotically quadratic convergence when using the system (3) also for bifurcation points, see e.g. Table I.

The direct procedure can be used as a suplement of a linear stability eigenvalue computation. It can be started from the undeformed initial state or from a path-following algorithm from an arbitrary state. In this case some indication of a forthcoming critical point can be obtained by monitoring the lowest eigenvalue or the determinant of the stiffness matrix.

An alternative approach is given by Cardona and Huespe [18, Eq. (29)], augmenting the bifurcation condition

$$\mathbf{p}_{\mathrm{r}}^T\boldsymbol{\phi} = 0 \tag{7}$$

into the extended system (3). Distinction between a limit and a bifurcation point has to be done during the iteration.

2.2. Polynomial eigenvalue problem

In this section consistent polynomial eigenvalue problem is formulated. Primary motivation is to show the connection to the full non-linear eigenvalue problem and to the asymptotic analysis [42].

Assuming an arbitrary equilibrium state $(\mathbf{q}_*, \lambda_*)$ with a regular tangent matrix, a Taylor expansion of the non-linear eigenvalue problem (1) with respect to the load parameter λ has the form

$$\mathbf{q} = \mathbf{q}_* + \Delta\lambda\mathbf{q}_1 + \tfrac{1}{2}(\Delta\lambda)^2\mathbf{q}_2 + \cdots, \tag{8}$$

$$\mathbf{f} = \mathbf{f}_* + \Delta\lambda\frac{\mathrm{d}\mathbf{f}}{\mathrm{d}\lambda}\bigg|_* + \frac{1}{2}(\Delta\lambda)^2\frac{\mathrm{d}^2\mathbf{f}}{\mathrm{d}\lambda^2}\bigg|_* + \cdots = \mathbf{0} \tag{9}$$

$$\left(\mathbf{f}'_* + \Delta\lambda\frac{\mathrm{d}\mathbf{f}'}{\mathrm{d}\lambda}\bigg|_* + \frac{1}{2}(\Delta\lambda)^2\frac{\mathrm{d}^2\mathbf{f}'}{\mathrm{d}\lambda^2}\bigg|_* + \cdots\right)\boldsymbol{\phi} = \mathbf{0} \tag{10}$$

where $\Delta\lambda = \lambda - \lambda_*$. Expressions for the derivatives are [‡]

$$\frac{\mathrm{d}\mathbf{f}}{\mathrm{d}\lambda} = \frac{\partial \mathbf{f}}{\partial \mathbf{q}}\frac{\partial \mathbf{q}}{\partial \lambda} + \frac{\partial \mathbf{f}}{\partial \lambda} = \mathbf{f}'\dot{\mathbf{q}} + \dot{\mathbf{f}}, \tag{11}$$

$$\frac{\mathrm{d}^2\mathbf{f}}{\mathrm{d}\lambda^2} = \mathbf{f}'\ddot{\mathbf{q}} + \mathbf{f}''\dot{\mathbf{q}}\dot{\mathbf{q}} + 2\dot{\mathbf{f}}'\dot{\mathbf{q}} + \ddot{\mathbf{f}}, \tag{12}$$

$$\frac{\mathrm{d}\mathbf{f}'}{\mathrm{d}\lambda} = \mathbf{f}''\dot{\mathbf{q}} + \dot{\mathbf{f}}', \tag{13}$$

$$\frac{\mathrm{d}^2\mathbf{f}'}{\mathrm{d}\lambda^2} = \mathbf{f}''\ddot{\mathbf{q}} + \mathbf{f}'''\dot{\mathbf{q}}\dot{\mathbf{q}} + 2\dot{\mathbf{f}}''\dot{\mathbf{q}} + \ddot{\mathbf{f}}'. \tag{14}$$

Evaluating these quantities at the equilibrium state $(\mathbf{q}_*, \lambda_*)$, gives

$$\dot{\mathbf{q}}_* = \mathbf{q}_1, \quad \text{and} \quad \ddot{\mathbf{q}}_* = \mathbf{q}_2, \quad \text{etc..} \tag{15}$$

and the expressions (11)-(14) result in

$$\left.\frac{\mathrm{d}\mathbf{f}}{\mathrm{d}\lambda}\right|_* = \mathbf{f}'_*\mathbf{q}_1 + \dot{\mathbf{f}}_*, \tag{16}$$

$$\left.\frac{\mathrm{d}\mathbf{f}'}{\mathrm{d}\lambda}\right|_* = \mathbf{f}''_*\mathbf{q}_1 + \dot{\mathbf{f}}'_*, \tag{17}$$

$$\left.\frac{\mathrm{d}^2\mathbf{f}}{\mathrm{d}\lambda^2}\right|_* = \mathbf{f}'_*\mathbf{q}_2 + \mathbf{f}''_*\mathbf{q}_1\mathbf{q}_1 + 2\dot{\mathbf{f}}'_*\mathbf{q}_1 + \ddot{\mathbf{f}}_*, \tag{18}$$

$$\left.\frac{\mathrm{d}^2\mathbf{f}'}{\mathrm{d}\lambda^2}\right|_* = \mathbf{f}''_*\mathbf{q}_2 + \mathbf{f}'''_*\mathbf{q}_1\mathbf{q}_1 + 2\dot{\mathbf{f}}''_*\mathbf{q}_1 + \ddot{\mathbf{f}}'_*, \tag{19}$$

where $\mathbf{f}_* = \mathbf{f}(\mathbf{q}_*, \lambda_*)$ etc. In the expansion of the equilibrium equations (9) all terms $\mathrm{d}^p\mathbf{f}/\mathrm{d}\lambda^p, p = 1, 2, \ldots$ has to vanish, thus giving the equation to solve the fields $\mathbf{q}_i$

$$\mathbf{f}'_*\mathbf{q}_1 = -\dot{\mathbf{f}}_*, \tag{20}$$

$$\mathbf{f}'_*\mathbf{q}_2 = -\left[\mathbf{f}''_*\mathbf{q}_1\mathbf{q}_1 + 2\dot{\mathbf{f}}'_*\mathbf{q}_1 + \ddot{\mathbf{f}}_*\right], \quad \ldots \quad \text{etc.} \tag{21}$$

It is worthwhile to notice that the coefficent matrix to solve $\mathbf{q}_1, \mathbf{q}_2 ...$ is the same for all the cases (20), (21) etc. In structural mechanics, the symbol $\mathbf{K}$ is usually used to denote the stiffness matrix, thus the matrices in (10) can be written as

$$\mathbf{K}_{0|*} = \mathbf{f}'_*, \tag{22}$$

$$\mathbf{K}_{1|*} = \left.\frac{\mathrm{d}\mathbf{f}}{\mathrm{d}\lambda}\right|_* = \mathbf{f}''_*\mathbf{q}_1 + \dot{\mathbf{f}}'_*, \tag{23}$$

$$\mathbf{K}_{2|*} = \left.\frac{\mathrm{d}^2\mathbf{f}}{\mathrm{d}\lambda^2}\right|_* = \mathbf{f}''_*\mathbf{q}_2 + \mathbf{f}'''_*\mathbf{q}_1\mathbf{q}_1 + 2\dot{\mathbf{f}}''_*\mathbf{q}_1 + \ddot{\mathbf{f}}'_*, \tag{24}$$

and the polynomial eigenvalue problem can be written as

$$\left(\mathbf{K}_{0|*} + \Delta\lambda\mathbf{K}_{1|*} + \tfrac{1}{2}(\Delta\lambda)^2\mathbf{K}_{2|*} + \cdots\right)\boldsymbol{\phi} = \mathbf{0}, \tag{25}$$

[‡]Notice the difference between derivatives $\mathrm{d}\mathbf{f}/\mathrm{d}\lambda$ and $\dot{\mathbf{f}} = \partial\mathbf{f}/\partial\lambda$, i.e. $\mathrm{d}\mathbf{f}/\mathrm{d}\lambda = \mathbf{f}'(\partial\mathbf{q}/\partial\lambda) + \partial\mathbf{f}/\partial\lambda$.

In the classical linear stability analysis the reference state is the undeformed stress free configuration. Assuming also dead weight loading, i.e. $\dot{\mathbf{f}}' \equiv \mathbf{0}$, the matrices for the linear stability eigenvalue problem are simply the following:

$$\mathbf{K}_{0|0} = \mathbf{f}'(\mathbf{0}, 0) \tag{26}$$

$$\mathbf{K}_{1|0} = \mathbf{f}''(\mathbf{0}, 0)\mathbf{q}_1, \tag{27}$$

where $\mathbf{K}_{0|0}\mathbf{q}_1 = \mathbf{p}_r$. Therefore the strains are linear functions of the displacements $\mathbf{q}_1$ and the geometric stiffness matrix $\mathbf{K}_{1|0}$ is a linear function of the displacements $\mathbf{q}_1$.

It is seen from the definition of the $\mathbf{K}_{1|0}$ matrix that the "initial stress" state to the linear eigenvalue problem has to be linear with respect to the load parameter change. This is not true if the linear stability eigenvalue problem is solved from

$$\big(\mathbf{K}_{0|*} + s(\mathbf{K}_{0|*} - \mathbf{K}_{0|**})\big)\,\boldsymbol{\phi} = \mathbf{0}, \tag{28}$$

where $\mathbf{K}_{0|*}$ and $\mathbf{K}_{0|**}$ are the tangent stiffness matrices from two consecutive equilibrium states. It will be a correct approximation to the consistently linearized eigenvalue problem only if the load increment $\Delta\lambda = \lambda_* - \lambda_{**}$ is small, i.e. $\mathbf{K}_{1|*} \approx (\Delta\lambda)^{-1}(\mathbf{K}_{0|*} - \mathbf{K}_{0|**})$.

2.3. Some computational issues

One bottleneck in applying the Newton's method to the extended system (3) or (6) is the need to compute the matrix $\mathbf{Z}$ or the vector $\mathbf{n}$ which requires evaluation of the second derivatives of the residual vector with respect to the state variables. If the iteration is started at the undeformed configuration, i.e. at $(\mathbf{q} = \mathbf{0}, \lambda = 0)$ the $\mathbf{Z}$ matrix is simply the initial stress or geometric stiffness matrix formed from the linearized stresses evaluated from a displacement field which is the initial guess of the eigenvector $\boldsymbol{\phi}$. This can be seen by comparing equations (5) and (27). A modified Newton scheme, where the $\mathbf{Z}$ matrix is not updated will completely avoid the evaluation of the second derivative terms. However, numerical experiments show that the rate of convergence can be extremely slow. The vector $\mathbf{n}$ is simply the load stiffness matrix multiplied with the eigenmode approximation.

If direct solvers for the solution of the linearized system is used, a block elimination scheme is a feasible choise. Denoting a general extended system (3) or (6) as

$$\begin{cases} \hat{\mathbf{f}}(\mathbf{q}, \lambda) := \mathbf{f}(\mathbf{q}, \boldsymbol{\lambda}) + \mathbf{f}_0(\mathbf{q}, \boldsymbol{\lambda}) = \mathbf{0} \\ \mathbf{h}(\mathbf{q}, \boldsymbol{\phi}, \lambda) := \mathbf{f}'(\mathbf{q}, \boldsymbol{\lambda})\boldsymbol{\phi} + \mathbf{h}_0(\mathbf{q}, \boldsymbol{\lambda}) = \mathbf{0} \\ \mathbf{c}(\mathbf{q}, \boldsymbol{\phi}, \lambda) = \mathbf{0}, \end{cases} \tag{29}$$

where $\boldsymbol{\lambda}$ is a vector of control and auxiliary parameters and $\mathbf{c}$ is a vector of constraint equations, dimension of these vectors is $p \geq 1$. The additional stabilizing functions $\mathbf{f}_0$ and $\mathbf{h}_0$ are chosen such that $\mathbf{f}_0 = \mathbf{h}_0 = \mathbf{0}$ at the solution point. The Newton linearization step can be written as

$$\begin{bmatrix} \mathbf{K}_f & \mathbf{0} & \mathbf{P} \\ \mathbf{Z} & \mathbf{K}_h & \mathbf{N} \\ \mathbf{C}_q & \mathbf{C}_\phi & \mathbf{C}_\lambda \end{bmatrix} \begin{Bmatrix} \delta\mathbf{q} \\ \delta\boldsymbol{\phi} \\ \delta\boldsymbol{\lambda} \end{Bmatrix} = - \begin{Bmatrix} \hat{\mathbf{f}} \\ \mathbf{h} \\ \mathbf{c} \end{Bmatrix}, \tag{30}$$

where

$$\mathbf{K}_f = \mathbf{K} + \mathbf{f}_0', \quad \mathbf{K}_h = \mathbf{K} + \frac{\partial \mathbf{h}_0}{\partial \boldsymbol{\phi}}, \quad \mathbf{P} = \frac{\partial \hat{\mathbf{f}}}{\partial \boldsymbol{\lambda}} \quad \text{and} \quad \mathbf{N} = \frac{\partial \mathbf{h}}{\partial \boldsymbol{\lambda}} \tag{31}$$

Partitioning the iterative steps $\delta\mathbf{q}$ and $\delta\boldsymbol{\phi}$ as

$$\delta\mathbf{q} = \mathbf{q}_f + \mathbf{Q}_p\delta\boldsymbol{\lambda}, \quad \delta\boldsymbol{\phi} = \boldsymbol{\phi}_h + \boldsymbol{\Phi}_n\delta\boldsymbol{\lambda}, \tag{32}$$

where the vectors $\mathbf{q}_f, \boldsymbol{\phi}_h$ and the $n \times p$ matrices $\mathbf{Q}_p, \boldsymbol{\Phi}_g$ can be solved from equations

$$\mathbf{K}_f\mathbf{q}_f = -\hat{\mathbf{f}}, \tag{33}$$

$$\mathbf{K}_f\mathbf{Q}_p = -\mathbf{P}, \tag{34}$$

$$\mathbf{K}_h\boldsymbol{\phi}_h = -\mathbf{h} - \mathbf{Z}\mathbf{q}_{\mathrm{f}}, \tag{35}$$

$$\mathbf{K}_h\boldsymbol{\Phi}_n = -\mathbf{N} - \mathbf{Z}\mathbf{Q}_p. \tag{36}$$

The iterative change of the control parameters can be solved from the constraint conditions resulting in

$$\delta\boldsymbol{\lambda} = -(\mathbf{C}_\lambda + \mathbf{C}_q\mathbf{Q}_p + \mathbf{C}_\phi\boldsymbol{\Phi}_n)^{-1}(\mathbf{c} + \mathbf{C}_q\mathbf{q}_f + \mathbf{C}_\phi\boldsymbol{\phi}_h). \tag{37}$$

The specific choice in (6) yields $\mathbf{K}_h = \mathbf{K}_f$, which is computationally very attractive if a direct linear solver is used. However, if the matrices $\mathbf{K}_h$ and $\mathbf{K}_f$ do not differ too much, preconditioned iterative linear solvers can be used effectively. Solution of the augmented system (30) by the block elimination method requires factorization of one matrix of order n, reductions and backsubstitutions of $2(1 + p)$ r.h.s.-vectors. An alternative scheme suitable for the use of iterative linear solvers is decribed in [43], which operates directly with (29), but the preconditioner is set up in a block form and the incomplete factorization (or some other preconditioner) need to be computed only for the standard stiffness matrix.

The direct algorithm for the critical point search is based on the Newton's method which is locally convergent. According to the Kantorovich theorem [39, 40] the Newton sequence, starting at the initial point $\mathbf{x}_0$ converges to a unique solution if the following conditions are met: (i) $\mathbf{g}$ is continuously differentiable in a ball $\mathcal{B}(\mathbf{x}_0, r), r > 0$, (ii) the Jacobian matrix $\mathbf{g}'$ is nonsingular at $\mathbf{x}_0$ and $\|\mathbf{g}'(\mathbf{x}_0)^{-1}\| \leq \beta$, (iii) the Jacobian matrix is Lipschitz continuous in $\mathcal{B}(\mathbf{x}_0, r)$ with a Lipschitz constant γ, (iv) the first Newton step is sufficiently small, $\|\mathbf{g}'(\mathbf{x}_0)^{-1}\mathbf{g}(\mathbf{x}_0)\| \leq \eta$. Then, if $h_0 = \beta\gamma\eta < \frac{1}{2}$, the solution is in $\mathcal{B}(\mathbf{x}_0, r_1)$, where $r_1 = \min(r, r_0)$, and $r_0 \equiv (1 - \sqrt{1 - 2h_0})/\beta\gamma$. The initial step can be made small, however, the crucial point is the Lipshitz constant γ, which can be large and the method does not converge.

On the other hand the indirect method is globally convergent, and combining the direct critical point search algorithm with a continuation algorithm could improve its usefulness.

Comparison of computational costs between the direct and indirect methods depend largely on the problem at hand. In general, it could be of same order, if the incrementation in the indirect method is done in a reasonable way. The indirect procedure is not designed for very accurate determination of the critical load, in contrast to the direct method.

The direct critical point search algorithm converges usually to the closest critical point along the equilibrium path. However, if the prediction step is large, convergence to a second critical point could occur. To avoid wrong decisions, it is advisable to monitore the sign of the lowest eigenvalue estimate of the stiffness matrix during the iterates. Computation of the inertia of the stiffness matrix at the critical point will make sure if convergence to a correct critical point has been obtained. This can be done easily if a direct linear solver is used.

2.4. On the constraint equations

In this study the following constraint forms have been compared

$$c(\boldsymbol{\phi}, \lambda) := \|\boldsymbol{\phi}\|^2 - 1 = 0, \tag{38}$$

$$c(\boldsymbol{\phi}, \lambda) := \lambda\|\boldsymbol{\phi}\|^2 - 1 = 0, \tag{39}$$

$$c(\boldsymbol{\phi}, \lambda) := \mathbf{e}_i^{\mathrm{T}}\boldsymbol{\phi} - 1 = 0, \tag{40}$$

$$c(\boldsymbol{\phi}, \lambda) := \lambda(\mathbf{e}_i^{\mathrm{T}}\boldsymbol{\phi})^2 - 1 = 0. \tag{41}$$

The constraint type (40) is used by Wriggers and Simo [17], see eq. (6), where it has now been chosen $\phi_0 = 1$. Constraints (39) and (41) guarantees that the iteration will converge to a solution with a positive critical value of the load parameter λ.

A proper scaling of the constraint equation is also important. Especially for the constraint equation (39) the best numerical performance is obtained when the initial scaling of the eigenvector approximation is of order $\|\boldsymbol{\phi}\| \sim \lambda_{\mathrm{cr}}^{-1}$.

3. GEOMETRICALLY EXACT BEAM MODEL

In this section a brief summary to the derivation of a geometrically exact Reissner's beam model based on total Lagrangian approach is given mainly to facilitate understanding the derivation of the $\mathbf{Z}$ matrix. For detailed exposition the reader is referred to [30].

3.1. Description of rotation

A rotation motion can be represented by rotation operators $\mathbf{R}$ forming a special noncommutative Lie-group of the proper orthogonal linear transformations, which is defined as

$$SO(3) := \left\{ \mathbf{R} : \mathsf{E}^3 \to \mathsf{E}^3 \,\middle|\, \mathbf{R}^{\mathrm{T}}\mathbf{R} = \mathbf{I},\ \det \mathbf{R} = +1 \right\}, \tag{42}$$

where E^3 denotes the 3-dimensional Euclidean vector space. The rotation tensor can be represented minimally by three parameters, which parametrize rotation tensor only locally. It is well known that there exist no a single three-parametric global presentation of rotation tensor because the rotation group is a compact group. The rotation operator $\mathbf{R}$ can be written in terms of the rotation vector that is defined by $\boldsymbol{\Psi} := \psi\mathbf{n}$, $\mathbf{n} \in \mathsf{E}^3, \psi \in \mathsf{R}_+$. This yields the expression of the rotation operator

$$\mathbf{R} := \mathbf{I} + \frac{\sin\psi}{\psi}\tilde{\boldsymbol{\Psi}} + \frac{1-\cos\psi}{\psi^2}\tilde{\boldsymbol{\Psi}}^2 = \exp(\tilde{\boldsymbol{\Psi}}), \quad \psi = \|\boldsymbol{\Psi}\|, \tag{43}$$

where the skew-symmetric rotation tensor $\tilde{\boldsymbol{\Psi}}$, is defined formally $\tilde{\boldsymbol{\Psi}} := \boldsymbol{\Psi}\times$. Compound rotation can be defined by two different, nevertheless, equivalent ways: the material description, and the spatial description. The material description of a compound rotation is defined as

$$\mathbf{R}\mathbf{R}_{\mathrm{inc}}^{\mathrm{mat}} = \mathbf{R}\exp(\tilde{\boldsymbol{\Theta}}) \quad \mathbf{R}_{\mathrm{inc}}^{\mathrm{mat}}, \mathbf{R} \in SO(3), \tag{44}$$

where $\mathbf{R}_{\mathrm{inc}}^{\mathrm{mat}}$ is an incremental material rotation operator, and $\boldsymbol{\Theta}$ is an incremental material rotation vector with respect to the base point $\mathbf{R} \in SO(3)$. This description is called material, since the incremental rotation operator acts on a material vector space. Differentiating the

material expression of the compound rotation $\mathbf{R}\exp(\eta\,\tilde{\mathbf{\Theta}})$ with respect to the parameter η and setting $\eta = 0$, yields the material tangent space at the base point $\mathbf{R} \in SO(3)$, defined as

$$ {}_{\mathrm{mat}}T_{\mathbf{R}}SO(3) := \{\tilde{\mathbf{\Theta}}_{\mathbf{R}} := (\mathbf{R}, \tilde{\mathbf{\Theta}}) \mid \text{for any } \ \tilde{\mathbf{\Theta}} \in so(3)\}, \tag{45} $$

where the skew-symmetric tensor $\tilde{\mathbf{\Theta}}_{\mathbf{R}} \in {}_{\mathrm{mat}}T_{\mathbf{R}}SO(3)$ is an element of the material tangent space and $so(3)$ denotes the Lie algebra. The notation $(\mathbf{R}, \tilde{\mathbf{\Theta}})$, the pair of the rotation operator $\mathbf{R}$ and the skew-symmetric tensor $\tilde{\mathbf{\Theta}}$, represents the material skew-symmetric tensor at the base point $\mathbf{R} \in SO(3)$. Considering the material form of a compound rotation (44), with the aid of η-parametrized exponential mappings

$$ \exp(\tilde{\mathbf{\Psi}} + \eta\,\delta\tilde{\mathbf{\Psi}}) = \exp(\tilde{\mathbf{\Theta}})\exp(\eta\,\delta\tilde{\mathbf{\Theta}}_{\mathbf{R}}) \tag{46} $$

where we are finding an incremental rotation tensor, the virtual rotation tensor $\delta\tilde{\mathbf{\Psi}}$, such that it belongs to the same tangent space as the rotation tensor $\tilde{\mathbf{\Psi}}$, i.e. such that $\delta\tilde{\mathbf{\Psi}}, \tilde{\mathbf{\Psi}} \in {}_{\mathrm{mat}}T_{\mathbf{I}}SO(3)$ with the identity as a base point omitted for simplicity. Taking the derivative of (46) with respect to the parameter η at $\eta = 0$ gives

$$ \delta\tilde{\mathbf{\Theta}}_{\mathbf{R}} = \mathbf{T}\cdot\delta\tilde{\mathbf{\Theta}} \tag{47} $$

$$ \mathbf{T} := \frac{\sin\psi}{\psi}\mathbf{I} - \frac{1-\cos\psi}{\psi^2}\tilde{\mathbf{\Psi}} + \frac{\psi-\sin\psi}{\psi^3}\mathbf{\Psi}\otimes\ \mathbf{\Psi} \tag{48} $$

$$ \psi := \|\mathbf{\Psi}\|, \quad \mathbf{R} = \exp(\tilde{\mathbf{\Psi}}), \quad \lim_{\mathbf{\Psi}\to\mathbf{0}} \mathbf{T}(\mathbf{\Psi}) = \mathbf{I} \tag{49} $$

where the material tangential transformation $\mathbf{T} = \mathbf{T}(\mathbf{\Psi})$ is a linear mapping between the virtual material tangent spaces: ${}_{\mathrm{mat}}T_{\mathbf{I}}SO(3) \ \rightarrow \ {}_{\mathrm{mat}}T_{\mathbf{R}}SO(3)$. The virtual incremental rotation vector $\delta\mathbf{\Theta}_{\mathbf{R}}$ and the virtual total rotation vector $\delta\mathbf{\Psi}$ belong to different vector spaces on the manifold, since the tangential transformation $\mathbf{T}$ is equal to the identity only at $\mathbf{\Psi} = \mathbf{0}$. Note that the transformation $\mathbf{T}$ has an effect on the base points, changing the base point $\mathbf{I}$ into $\mathbf{R}$. For convenience, a material vector space on the rotation manifold at any point $\mathbf{R}$ is defined as

$$ {}_{\mathrm{mat}}T_{\mathbf{R}} := \left\{ \mathbf{\Theta}_{\mathbf{R}} \in \mathsf{E}^3 \;\middle|\; \tilde{\mathbf{\Theta}}_{\mathbf{R}} \in {}_{\mathrm{mat}}T_{\mathbf{R}}SO(3) \right\} \tag{50} $$

where an element of the material vector space is $\mathbf{\Theta}_{\mathbf{R}} \in {}_{\mathrm{mat}}T_{\mathbf{R}}$, which is an affine space with the rotation vector $\mathbf{\Psi}$ as a base point and the incremental rotation vector $\mathbf{\Theta}$ as a tangent vector, then $\mathbf{T} : {}_{\mathrm{mat}}T_{\mathbf{I}} \rightarrow {}_{\mathrm{mat}}T_{\mathbf{R}}$. Definition (50) gives a practical notation for sorting rotation vectors in different tangent spaces.

3.2. Virtual work expression for the Reissner's beam model

In the material representation, the internal virtual work expression for the Reissner's beam model is

$$ \delta W_{\mathrm{int}} = \int_L (\delta\mathbf{\Gamma}\cdot\mathbf{N} + \delta\mathbf{K}_{\mathbf{R}}\cdot\mathbf{M}_{\mathbf{R}})\,\mathrm{d}s, \tag{51} $$

where the material curvature tensor is defined by $\tilde{\mathbf{K}}_{\mathbf{R}} := \mathbf{R}^{\mathrm{T}}\mathbf{R}'$, and the prime denotes derivative with respect to the coordinate s along the beam's axis. The material internal force vector $\mathbf{N}$ and the material internal moment vector $\mathbf{M}_{\mathbf{R}}$ are related to the material strain and curvature vectors by a linear constitutive law

$$ \mathbf{N} = \mathbf{C}_{\mathrm{N}}\mathbf{\Gamma}, \quad \mathbf{M}_{\mathbf{R}} = \mathbf{C}_{\mathrm{M}}\mathbf{K}_{\mathbf{R}}. \tag{52} $$

The work conjugate of the material vector $\mathbf{N}$ is the variation of the material strain vector $\mathbf{\Gamma}$, defined by the formula and its variation:

$$\mathbf{\Gamma} := \mathbf{R}^{\mathrm{T}}\mathbf{x'}_{\mathrm{c}} - \mathbf{E}_1, \quad \delta\mathbf{\Gamma} = \mathbf{R}^{\mathrm{T}}\delta\mathbf{x'}_{\mathrm{c}} - \delta\tilde{\mathbf{\Theta}}\mathbf{R}^{\mathrm{T}}\mathbf{x'}_{\mathrm{c}}, \tag{53}$$

where the vector $\mathbf{x}_{\mathrm{c}}$ defines the center line of tbe beam's cross-section and $\mathbf{E}_1$ is a Cartesian material base vector, see Section 3.1 in Ref. [30]. In the total Lagrangian formulation, the virtual work expression has to be written in terms of the total material rotation vector $\mathbf{\Psi}$ and its virtual counterpart $\delta\mathbf{\Psi}$. The virtual work of the internal forces (51) has the form

$$\delta W_{\mathrm{int}} = \int_L (\delta\mathbf{x'}_{\mathrm{c}} \cdot \mathbf{RN})\,\mathrm{d}s + \int_L (\delta\mathbf{\Psi} \cdot (-\mathbf{T}^{\mathrm{T}}\widetilde{\mathbf{R}^{\mathrm{T}}\mathbf{x'}_{\mathrm{c}}}\mathbf{N} + \mathbf{C}_1^{\mathrm{T}}(\mathbf{\Psi'}, \mathbf{\Psi})\,\mathbf{M_R}) + \delta\mathbf{\Psi'} \cdot \mathbf{T}^{\mathrm{T}}\mathbf{M_R})\,\mathrm{d}s, \tag{54}$$

where the tensor $\mathbf{C}_1$ is given in the Appendix. The internal virtual work can be written compactly as

$$\delta W_{\mathrm{int}} = \int_L \delta\hat{\mathbf{q}} \cdot \mathbf{B}^{\mathrm{T}}\mathbf{F}_{\mathrm{int}}\,\mathrm{d}s, \tag{55}$$

where $\delta\hat{\mathbf{q}} := (\delta\mathbf{x'}_{\mathrm{c}}, \delta\mathbf{\Psi'}, \delta\mathbf{\Psi})$. The generalized internal force field $\mathbf{F}_{\mathrm{int}}$ and the kinematic tensor $\mathbf{B}$ are

$$\mathbf{F}_{\mathrm{int}} := \begin{pmatrix} \mathbf{N} \\ \mathbf{M_R} \end{pmatrix}, \quad \mathbf{B} := \begin{pmatrix} \mathbf{R}^{\mathrm{T}} & \mathbf{O} & \widetilde{\mathbf{R}^{\mathrm{T}}\mathbf{x'}_{\mathrm{c}}}\mathbf{T} \\ \mathbf{O} & \mathbf{T} & \mathbf{C}_1(\mathbf{\Psi'}, \mathbf{\Psi}) \end{pmatrix}. \tag{56}$$

Moreover, the field $\mathbf{F}_{\mathrm{int}}$ can be given in the term of the material strain and curvature vectors with the aid of the constitutive relations (52). Linearizing the internal work form δW_{int} at the point $\mathbf{q}_0^{\mathrm{T}} = (\mathbf{d}_0^{\mathrm{T}}, \mathbf{\Psi}_0^{\mathrm{T}})$ in the vector direction $\Delta\hat{\mathbf{q}}^{\mathrm{T}} = (\Delta\mathbf{x'}_{\mathrm{c}}^{\mathrm{T}}, \Delta\mathbf{\Psi'}^{\mathrm{T}}, \Delta\mathbf{\Psi}^{\mathrm{T}})$ will result in the equation

$$\mathrm{Lin}\,(\delta W_{\mathrm{int}}(\mathbf{q}; \delta\hat{\mathbf{q}})) = \delta W_{\mathrm{int}}(\mathbf{q}_0; \delta\hat{\mathbf{q}}) + \mathrm{D}_{\mathbf{q}}\delta W_{\mathrm{ext}}(\mathbf{q}_0, \delta\hat{\mathbf{q}}) \cdot \Delta\hat{\mathbf{q}}, \tag{57}$$

where the linear form $\mathrm{D}_{\hat{\mathbf{q}}}\delta W_{\mathrm{int}} \cdot \Delta\hat{\mathbf{q}}$ can be written using the material stiffness tensor $\mathbf{K}_{\mathrm{mat}}$ and the geometric stiffness tensor $\mathbf{K}_\sigma$ as

$$\mathrm{D}_{\hat{\mathbf{q}}}\delta W_{\mathrm{int}} \cdot \Delta\hat{\mathbf{q}} = \int_L (\mathbf{K}_{\mathrm{mat}} + \mathbf{K}_\sigma) \,:\, (\delta\hat{\mathbf{q}} \otimes \Delta\hat{\mathbf{q}})\,\mathrm{d}s, \quad \mathbf{K}_{\mathrm{mat}} := \mathbf{B}_0^{\mathrm{T}}\mathbf{C}_{\mathrm{NM}}\mathbf{B}_0, \tag{58}$$

$$\mathbf{K}_\sigma := \begin{pmatrix} \mathbf{O} & \mathbf{O} & -\mathbf{R}\tilde{\mathbf{N}}\mathbf{T} \\ \mathbf{O} & \mathbf{O} & \mathbf{C}_2(\mathbf{M_R}, \mathbf{\Psi}_0) \\ \mathbf{T}^{\mathrm{T}}\tilde{\mathbf{N}}\mathbf{R}^{\mathrm{T}} & \mathbf{C}_2^{\mathrm{T}}(\mathbf{M_R}, \mathbf{\Psi}_0) & \mathbf{K}_{\sigma 33} \end{pmatrix}, \quad \text{where}$$

$$\mathbf{K}_{\sigma 33} = \mathbf{C}_3(\mathbf{M_R}, \mathbf{\Psi'}_0, \mathbf{\Psi}_0) + \mathbf{C}_2(\tilde{\mathbf{N}}\mathbf{R}^{\mathrm{T}}\mathbf{x'}_{\mathrm{c}}, \mathbf{\Psi}_0) + \mathbf{T}^{\mathrm{T}}\tilde{\mathbf{N}}\widetilde{\mathbf{R}^{\mathrm{T}}\mathbf{x'}_{\mathrm{c}}}\mathbf{T}. \tag{59}$$

The material stiffness tensor $\mathbf{K}_{\mathrm{mat}}$ arises from the linearization of the vector $\mathbf{F}_{\mathrm{int}}$ with the aid of kinematic relation, and the geometric stiffness tensor $\mathbf{K}_\sigma$ arises from the linearization of the kinematic operator $\mathbf{B}$. The tensors $\mathbf{C}_2$ and $\mathbf{C}_3$ are given in the Appendix. Note that the material stiffness tensor $\mathbf{K}_{\mathrm{mat}}$ is symmetric due to the symmetry of the elasticity tensor $\mathbf{C}_{\mathrm{NM}}$. In addition, the geometric stiffness $\mathbf{K}_\sigma$ is also a symmetric tensor. This symmetry of the stiffness tensor is due to the local parametrization of the rotation operator.

3.3. Expressions for the second derivatives of the residual

The **Z**-matrix in the Jacobian (4) of the extended system (3) is a sum of the following two matrices defined as

$$\int_L \mathbf{Z}_{\mathrm{mat}}\,\mathrm{d}s := \int_L \mathrm{D}_{\hat{\mathbf{q}}}\mathbf{K}_{\mathrm{mat}}\hat{\boldsymbol{\phi}}\,\mathrm{d}s = \int_L \mathrm{D}_{\hat{\mathbf{q}}}\mathbf{B}^{\mathrm{T}}\mathbf{C}\mathbf{B}\hat{\boldsymbol{\phi}}\,\mathrm{d}s, \tag{60}$$

$$\int_L \mathbf{Z}_{\sigma}\,\mathrm{d}s := \int_L \mathrm{D}_{\hat{\mathbf{q}}}\mathbf{K}_{\sigma}\hat{\boldsymbol{\phi}}\,\mathrm{d}s. \tag{61}$$

Partitioning the eigenvector $\hat{\phi}$ similarly as the displacement vector $\hat{\mathbf{q}}$: $\hat{\boldsymbol{\phi}}^{\mathrm{T}} := [\boldsymbol{\phi}_1^{\mathrm{T}}, \boldsymbol{\phi}_2^{\mathrm{T}}, \boldsymbol{\phi}_3^{\mathrm{T}}] \sim \hat{\mathbf{q}}^{\mathrm{T}} := [\mathbf{x'}_{\mathrm{c}}^{\mathrm{T}}, \boldsymbol{\Psi'}^{\mathrm{T}}, \boldsymbol{\Psi}^{\mathrm{T}}]$, the matrices $\mathbf{Z}_{\mathrm{mat}}$ and $\mathbf{Z}_{\sigma}$ have expressions

$$\mathbf{Z}_{\mathrm{mat}} = \mathbf{K}_{\sigma}(\mathbf{C}_{\mathrm{NM}}\mathbf{B}\hat{\boldsymbol{\phi}}) + \\ + \mathbf{B}^{\mathrm{T}}\mathbf{C}_{\mathrm{NM}}\begin{bmatrix} -\widetilde{\mathbf{T}\boldsymbol{\phi}_3}\mathbf{R}^{\mathrm{T}} & \mathbf{O} & \widetilde{\mathbf{R}^{\mathrm{T}}\boldsymbol{\phi}_1}\mathbf{T} + \widetilde{\mathbf{R}^{\mathrm{T}}\mathbf{x'}_{\mathrm{c}}}\mathbf{C}_1(\boldsymbol{\phi}_3,\boldsymbol{\Psi}) - \widetilde{\mathbf{T}\boldsymbol{\phi}_3}\widetilde{\mathbf{R}^{\mathrm{T}}\mathbf{x'}_{\mathrm{c}}}\mathbf{T} \\ \mathbf{O} & \dot{\mathbf{T}}(\boldsymbol{\phi}_3,\boldsymbol{\Psi}) & \mathbf{C}_1(\boldsymbol{\phi}_2,\boldsymbol{\Psi}) + \mathbf{C}_8(\boldsymbol{\phi}_3,\boldsymbol{\Psi}',\boldsymbol{\Psi}) \end{bmatrix}, \tag{62}$$

and

$$\mathbf{Z}_{\sigma} = \begin{bmatrix} \mathbf{O} & \mathbf{O} & \widetilde{\mathbf{R}\tilde{\mathbf{N}}\mathbf{T}\boldsymbol{\phi}_3}\mathbf{T} - \mathbf{R}\tilde{\mathbf{N}}\mathbf{C}_1(\boldsymbol{\phi}_3,\boldsymbol{\Psi}) \\ \mathbf{O} & \mathbf{O} & \mathbf{C}_7(\boldsymbol{\phi}_3,\mathbf{M},\boldsymbol{\Psi}) \\ \dot{\mathbf{T}}^{\mathrm{T}}(\boldsymbol{\phi}_3,\boldsymbol{\Psi})\tilde{\mathbf{N}}\mathbf{R}^{\mathrm{T}} & \mathbf{C}_9(\boldsymbol{\phi}_3,\mathbf{M},\boldsymbol{\Psi}) & \mathbf{Z}_{\sigma 33} \end{bmatrix} + \mathbf{Z}_{\mathrm{NM}}, \tag{63}$$

where

$$\mathbf{Z}_{\sigma 33} = \mathbf{T}^{\mathrm{T}}\tilde{\mathbf{N}}\widetilde{\mathbf{R}^{\mathrm{T}}\boldsymbol{\phi}_1}\mathbf{T} + \mathbf{C}_1(\tilde{\mathbf{N}}\widetilde{\mathbf{R}^{\mathrm{T}}\boldsymbol{\phi}_1},\boldsymbol{\Psi}) + \mathbf{C}_3(\mathbf{M},\boldsymbol{\phi}_2,\boldsymbol{\Psi}) + \mathbf{C}_{10}(\boldsymbol{\phi}_3,\mathbf{M},\boldsymbol{\Psi}',\boldsymbol{\Psi}) + \dot{\mathbf{T}}^{\mathrm{T}}(\boldsymbol{\phi}_3,\boldsymbol{\Psi})\tilde{\mathbf{N}}\widetilde{\mathbf{R}^{\mathrm{T}}\mathbf{x'}_{\mathrm{c}}}\mathbf{T} + \\ + \mathbf{C}_7(\boldsymbol{\phi}_3,\tilde{\mathbf{N}}\mathbf{R}^{\mathrm{T}}\mathbf{x'}_{\mathrm{c}},\boldsymbol{\Psi}) + \mathbf{C}_2(\tilde{\mathbf{N}}\widetilde{\mathbf{R}^{\mathrm{T}}\mathbf{x'}_{\mathrm{c}}}\mathbf{T}\boldsymbol{\phi}_3,\boldsymbol{\Psi}) - \mathbf{T}^{\mathrm{T}}\tilde{\mathbf{N}}\widetilde{\mathbf{T}\boldsymbol{\phi}_3}\widetilde{\mathbf{R}^{\mathrm{T}}\mathbf{x'}_{\mathrm{c}}}\mathbf{T} + \mathbf{T}^{\mathrm{T}}\tilde{\mathbf{N}}\widetilde{\mathbf{R}^{\mathrm{T}}\mathbf{x'}_{\mathrm{c}}}\mathbf{C}_1(\boldsymbol{\phi}_3,\boldsymbol{\Psi}) \tag{64}$$

and

$$\mathbf{Z}_{\mathrm{NM}} = \begin{bmatrix} \mathbf{R}\widetilde{\mathbf{T}\boldsymbol{\phi}_3} & \mathbf{O} \\ \mathbf{O} & \dot{\mathbf{T}}^{\mathrm{T}}(\boldsymbol{\phi}_3,\boldsymbol{\Psi}) \\ \mathbf{Z}_{\mathrm{NM31}} & \dot{\mathbf{T}}^{\mathrm{T}}(\boldsymbol{\phi}_2,\boldsymbol{\Psi}) + \mathbf{C}_8^{\mathrm{T}}(\boldsymbol{\phi}_3,\boldsymbol{\Psi}',\boldsymbol{\Psi}) \end{bmatrix}\mathbf{C}_{\mathrm{NM}}\mathbf{B}, \tag{65}$$

where

$$\mathbf{Z}_{\mathrm{NM31}} = -\mathbf{T}^{\mathrm{T}}\widetilde{\mathbf{R}^{\mathrm{T}}\boldsymbol{\phi}_1} - \dot{\mathbf{T}}^{\mathrm{T}}(\boldsymbol{\phi}_3,\boldsymbol{\Psi})\widetilde{\mathbf{R}^{\mathrm{T}}\mathbf{x'}_{\mathrm{c}}} - \mathbf{T}^{\mathrm{T}}\mathrm{skew}(\widetilde{\mathbf{R}^{\mathrm{T}}\mathbf{x'}_{\mathrm{c}}}\mathbf{T}\boldsymbol{\phi}_3). \tag{66}$$

It should be noted that the matrix **Z** is symmetric although the matrices $\mathbf{Z}_{\mathrm{mat}}$ and $\mathbf{Z}_{\sigma}$ are not.

4. NUMERICAL EXAMPLES

All the analyses have been performed in the Matlab environment on a PC. If not otherwise stated, the initial state for the critical point computation has been the equilibrium configuration corresponding to the reference load $\mathbf{p}_{\mathrm{r}}$.

It is noted that the initial value for the eigenvector $\boldsymbol{\phi}$ is chosen to be a vector for which one inverse power iteration is performed to a random vector. This considerably improves the likelihood for the iterates to find the domain of attraction of the Newton's scheme.

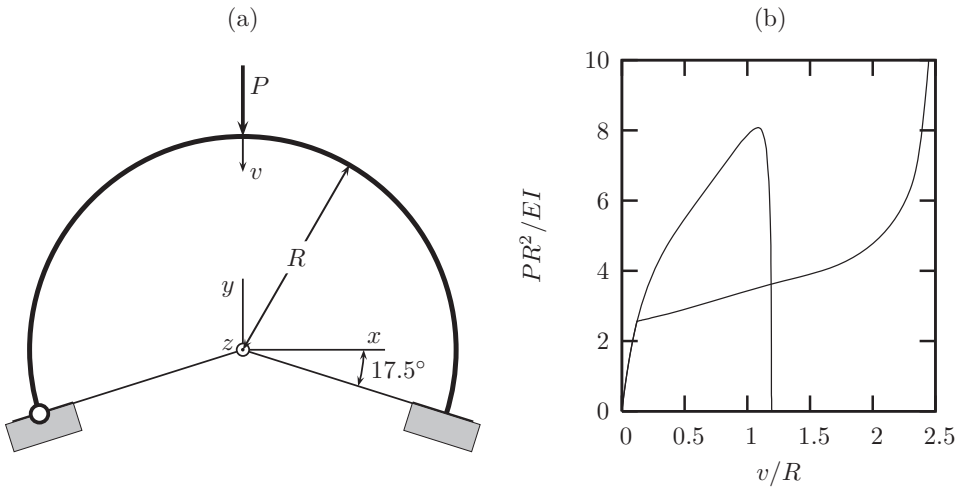

Figure 1. Deep circular arch: (a) geometry, (b) load-deflection curves.

4.1. Deep circular arch

A deep circular arch under vertical point load as shown in Figure 1a has been analysed. One support of the arch is clamped and the other is hinged allowing rotations about the $z-$axis. The same problem has also been analysed by Cardona and Huespe [18] and Battini et al. [12]. The problem data are: radius $R = 100$, Young's modulus $E = 6 \cdot 10^6$, Poisson's ratio $\nu = 0$, cross-sectional area $A = \sqrt{2}$, the double symmetric cross-section has flexural inertia $I = 1/6$ and torsional inertia $I_{\mathrm{t}} = 0.4741$.

The strucure is discretized by using 40 equal elements. Bifurcation point with out-of-plane deformations occur at the load level of 256.58 ($2.5658\ EI/R^2$). This value is in accordance to the results 256.5 and 256.7 obtained in Refs. [18, 12], respectively. If the out-of-plane displacements are prevented, the first critical point on the equilibrium path is a limit point at the load level of $8.076\ EI/R^2$. The load-deflection curves are shown in Figure 1b.

Consistently linearised buckling eigenvalue analysis, where the linearisation is performed with respect to the undeformed configuration, gives results 229.7 and 707.2 for the out-of-plane and in-plane buckling modes, respectively.

Convergence of the iteration towards the bifurcation point is shown in Table I using the constraint equation (38). The lowest eigenvalue of the stiffness matrix $\mathbf{K}$ is also tabulated. Similar convergence behaviour is obtained with the other constraints too. The load parameter λ is defined as $P = \lambda P_{\mathrm{ref}}$, where the reference load P_{ref} has the value 100. Although the Jacobian matrix of the extended system is singular, the iteration shows asymptotically quadratic convergence. The convergence is not affected of the element mesh.

If the starting point for the extended system is chosen to be an equilibrium point along the primary path closer to the critical point, the convergence will be faster. For example, starting from equilibrium points corresponding the load level of 100 or 200, six corrector iterations is required for similar accuracy as in Table I.

Table I. Deep circular arch, iteration to the bifurcation point.

it	λ	$\|\delta\mathbf{x}_i\|/\|\mathbf{x}_i\|$	$\|\mathbf{g}_i\|/\|\mathbf{g}_0\|$	lowest eigenvalue
0	1.0000	$3.2460{\cdot}10^{1}$	1.000	$1.4885{\cdot}10^{-1}$
1	2.7246	$1.0803{\cdot}10^{-1}$	$1.0967{\cdot}10^{3}$	$-3.5238{\cdot}10^{5}$
2	4.3356	$4.2092{\cdot}10^{-1}$	$4.2512{\cdot}10^{2}$	$-3.094{\cdot}10^{-1}$
3	2.5148	$2.7353{\cdot}10^{-2}$	$1.9850{\cdot}10^{2}$	$1.7580{\cdot}10^{0}$
4	2.4494	$1.1989{\cdot}10^{0}$	$3.3364{\cdot}10^{0}$	$6.5944{\cdot}10^{-3}$
5	2.5622	$2.7360{\cdot}10^{-2}$	$4.8727{\cdot}10^{2}$	$5.2051{\cdot}10^{0}$
6	1.9246	$6.4786{\cdot}10^{-2}$	$6.4027{\cdot}10^{1}$	$5.2660{\cdot}10^{-2}$
7	2.5712	$1.4306{\cdot}10^{-3}$	$5.6222{\cdot}10^{0}$	$1.5828{\cdot}10^{-1}$
8	2.5663	$4.7905{\cdot}10^{-4}$	$1.0582{\cdot}10^{-2}$	$2.9508{\cdot}10^{-4}$
9	2.5658	$5.6754{\cdot}10^{-6}$	$7.9740{\cdot}10^{-4}$	$9.7721{\cdot}10^{-6}$
10	2.5658	$3.4659{\cdot}10^{-8}$	$7.0583{\cdot}10^{-9}$	$3.7421{\cdot}10^{-9}$

4.2. Shallow hexagonal frame

Snap-through instability characterizes the large deformation behaviour of a shallow hexagonal dome under a point load, see Fig. 2. Horizontal movement of the supports can freely take place, except for two supports preventing the rigid-body motion. Ten elements in each member has been used. Tests using a plexiglas model of the frame has been conducted by Chu and Rampetsreiter [44]. The problem data are: Young's modulus $E = 3019.96$ MPa, Poisson's ratio $\nu = 0.383$, length $L = 609.6$ mm, height $H = 44.45$ mm, and the solid cross-section is a square having width $b = 17.78$ mm. The experimental limit load is 251 N [44] and the computed critical load is 251.16 N ($= 3.71\ EI/L^2$). In the unstable path there is a bifurcation point, marked by a star $\star$ in the Fig. 2b (solid line), where the number of unstable modes changes from one to three. The equilibrium path beyond this point has been computed with an extra horizontal support at the apex of the frame. Linear buckling eigenvalue analysis considerably overestimates the critical load giving the value 496.4 N.

If the horizontal movement of the supports is supressed, there is a double bifurcation point at the load level of 329.52 N ($4.87\ EI/L^2$), which is quite close to the symmetric snap trough point at the load level of 347.72 N ($5.14\ EI/L^2$). The load-deflection (of the apex) curves are shown in Fig.2b, where the path corresponding to the symmetric mode is drawn by using a solid line. The bifurcated solution in the case of fixed horizontal supports is indicated by a dashed line. To branch-out to the secondary path, the horizontal displacements of the apex are supressed, which changes the double bifurcation to a simple one.

For the horizontally free support case, convergence of the residual norm is shown in Fig. 3a when the constraints (38) or (39) is used and the reference load has the value 200 N. In Fig. 3b the effect of the reference load on the convergence behaviour is shown when the constraint (39) is used.

When the translational degrees of freedom of the supports are fixed, 9 or 10 iterations are needed to compute the bifurcation load. To obtain the symmetric limit load, the horizontal displacements and the rotation about the z-axis (load direction) need also to be prevented.

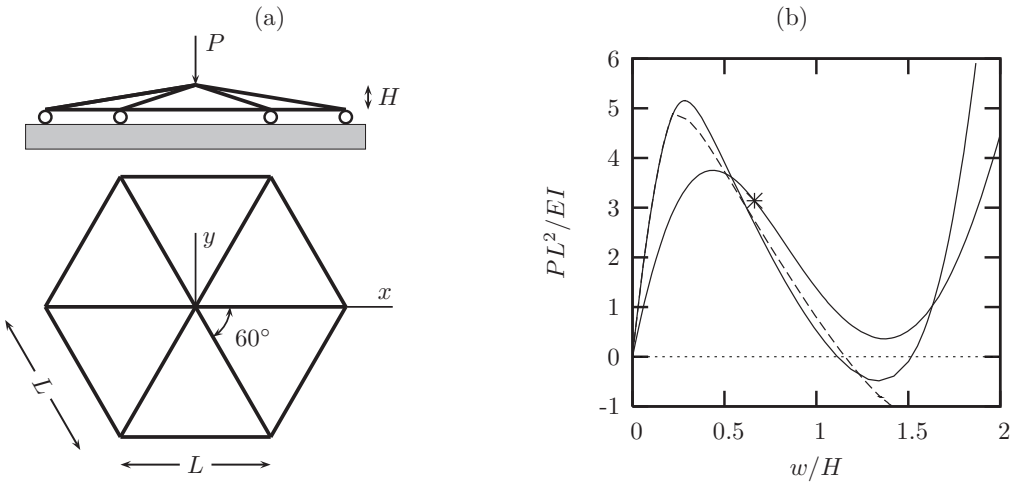

Figure 2. Shallow hexagonal dome: (a) geometry, (b) load-deflection curves.

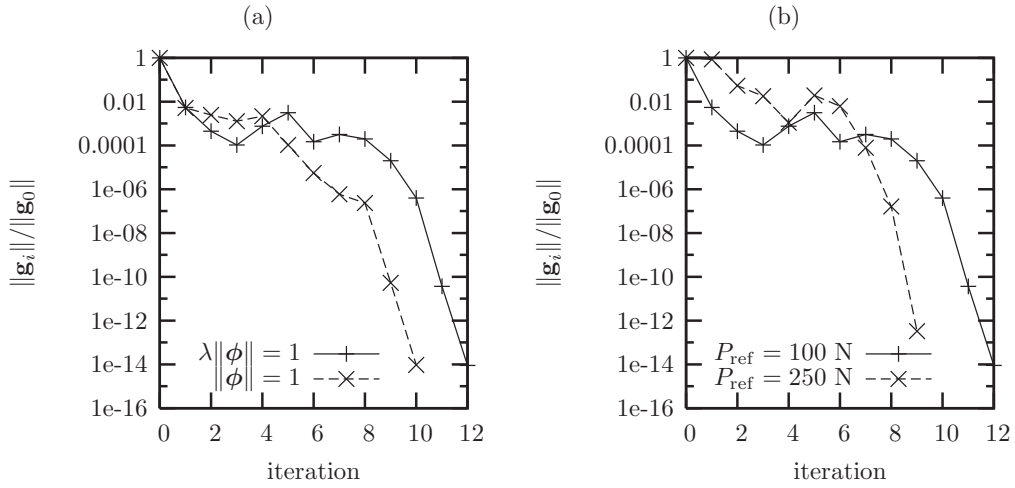

Figure 3. Shallow hexagonal dome: (a) convergence of the residual with the reference load 100 N, (b) effect of the reference load when using the constraint $\lambda\|\boldsymbol{\phi}\| = 1$.

Convergence to the limit point is very slow, see Tables II and III. Especially with the constraint (38) the iteration of the load parameter varies wildly, which also means difficulty in finding the critical equilibrium state. Using constraint (39) resulted in much more stable search of the critical point and quicker landing to the domain of attraction of the Newton's iteration.

Table II. Shallow hexagonal dome, iteration to the limit point, constraint eq. (38), $P_{\text{ref}} = 250$ N.

it	λ	$\|\delta\mathbf{x}_i\|/\|\mathbf{x}_i\|$	$\|\mathbf{g}_i\|/\|\mathbf{g}_0\|$	lowest eigenvalue
0	1.0000	$8.9628{\cdot}10^{0}$	1.000	$4.5798{\cdot}10^{-1}$
1	0.7204	$3.4202{\cdot}10^{-1}$	$9.4984{\cdot}10^{-1}$	$7.4501{\cdot}10^{-1}$
2	0.5068	$1.3037{\cdot}10^{1}$	$1.0179{\cdot}10^{-3}$	$8.9013{\cdot}10^{-1}$
3	6.2182	$1.3205{\cdot}10^{1}$	$1.0719{\cdot}10^{-2}$	$-1.9191{\cdot}10^{0}$
4	-3.7927	$3.9608{\cdot}10^{-1}$	$4.1498{\cdot}10^{-2}$	$-1.3475{\cdot}10^{0}$
5	-9.0675	$3.7702{\cdot}10^{-1}$	$8.6140{\cdot}10^{-2}$	$6.6085{\cdot}10^{0}$
6	35.675	$9.6723{\cdot}10^{-2}$	$8.1607{\cdot}10^{-2}$	$5.2991{\cdot}10^{0}$
7	51.810	$1.6575{\cdot}10^{-1}$	$1.2028{\cdot}10^{-2}$	$4.7198{\cdot}10^{0}$
8	13.709	$2.1833{\cdot}10^{-1}$	$1.2986{\cdot}10^{-2}$	$3.9776{\cdot}10^{0}$
9	-4.4952	$2.7880{\cdot}10^{-1}$	$7.8662{\cdot}10^{-3}$	$2.8676{\cdot}10^{0}$
10	-6.5095	$3.7858{\cdot}10^{-1}$	$5.7090{\cdot}10^{-3}$	$2.6612{\cdot}10^{-1}$
11	-1.5059	$4.7876{\cdot}10^{-1}$	$3.9036{\cdot}10^{-3}$	$-7.2658{\cdot}10^{-1}$
12	2.0222	$2.0170{\cdot}10^{-1}$	$5.6134{\cdot}10^{-3}$	$-1.6201{\cdot}10^{-1}$
13	1.7378	$8.9200{\cdot}10^{-2}$	$9.1679{\cdot}10^{-4}$	$-1.3976{\cdot}10^{-1}$
14	1.3641	$2.5113{\cdot}10^{-1}$	$4.5199{\cdot}10^{-5}$	$-1.1563{\cdot}10^{-1}$
15	1.4374	$1.0341{\cdot}10^{-1}$	$4.0270{\cdot}10^{-4}$	$9.4655{\cdot}10^{-2}$
16	1.4057	$5.9792{\cdot}10^{-3}$	$3.1477{\cdot}10^{-5}$	$-3.2353{\cdot}10^{-3}$
17	1.3909	$4.3012{\cdot}10^{-4}$	$6.5732{\cdot}10^{-8}$	$-2.7652{\cdot}10^{-4}$
18	1.3909	$8.8113{\cdot}10^{-8}$	$9.2565{\cdot}10^{-10}$	$6.3176{\cdot}10^{-8}$
19	1.3909	$5.0322{\cdot}10^{-13}$	$8.3283{\cdot}10^{-15}$	$1.2346{\cdot}10^{-10}$

4.3. Right-angle frame

Buckling behaviour of a clamped right-angle frame subjected to an end load is analyzed. The same problem has been computed also by Cardona and Huespe [18]. The material constants are: Young's modulus $E = 71.24$ GPa, Poisson's ratio $\nu = 0.31$, the solid rectangular cross-section has dimension 3.5 mm $\times$ 1.2 mm and the length $L = 240$ mm. Linear buckling eigenvalue analysis gives the results $P_{\text{cr}} = -0.8896\sqrt{EI_yGI_t}/L^2$ (-0.607 N) and $P_{\text{cr}} = 1.394\sqrt{EI_yGI_t}/L^2$ (0.951 N).

The critical loads obtained from the non-linear eigenvalue analysis when using 32 elements are $1.817\sqrt{EI_yGI_t}/L^2$ (1.2398 N) and $-0.977\sqrt{EI_yGI_t}/L^2$ (-0.666 N). The value reported by Cardona and Huespe is 1.241 N with 16 elements for the positive critical load. Some results from computations with different constraints (38) - (41) are shown in Table IV, where the iteration is terminated when $\|\mathbf{g}_i\| < 10^{-4}$. The non-linear eigenvalue iteration is started at the equilibrium point corresponding to the load level $P_* = 1$ N. If the starting point is as close as 1.2 N, four iterations for all constraints resulted in converged solution. In general the constraint (39) seems to be more robust than the others.

Results from computations with reversed load direction are shown in Table IV.

In addition also results with the stabilized extended system by Wriggers and Simo [17], equation (6), are shown in Table IV, where the value 100 has been used for the stabilization

Table III. Shallow hexagonal dome, iteration to the limit point, constraint eq. (39), $P_{\text{ref}} = 250$ N.

it	λ	$\|\delta\mathbf{x}_i\|/\|\mathbf{x}_i\|$	$\|\mathbf{g}_i\|/\|\mathbf{g}_0\|$	lowest eigenvalue
0	1.0000	$6.4307{\cdot}10^{-1}$	1.000	$4.5798{\cdot}10^{-1}$
1	1.1929	$1.0346{\cdot}10^{-1}$	$4.9948{\cdot}10^{-1}$	$2.8472{\cdot}10^{-1}$
2	1.2019	$4.0158{\cdot}10^{-1}$	$1.8573{\cdot}10^{-4}$	$2.6085{\cdot}10^{-1}$
3	1.4388	$6.5021{\cdot}10^{-1}$	$1.6777{\cdot}10^{-4}$	$7.8146{\cdot}10^{-2}$
4	1.5635	$3.8631{\cdot}10^{-1}$	$1.0746{\cdot}10^{-3}$	$-1.1814{\cdot}10^{-1}$
5	1.5072	$5.0365{\cdot}10^{-1}$	$7.2545{\cdot}10^{-4}$	$7.6428{\cdot}10^{-3}$
6	1.3757	$2.1996{\cdot}10^{-1}$	$1.0986{\cdot}10^{-3}$	$3.1678{\cdot}10^{-1}$
7	1.3456	$2.3921{\cdot}10^{-1}$	$5.5517{\cdot}10^{-4}$	$2.3432{\cdot}10^{-1}$
8	1.3719	$3.0290{\cdot}10^{-1}$	$5.7016{\cdot}10^{-5}$	$1.0943{\cdot}10^{-1}$
9	1.4500	$6.1929{\cdot}10^{-2}$	$2.0024{\cdot}10^{-4}$	$3.3836{\cdot}10^{-2}$
10	1.4224	$6.4150{\cdot}10^{-3}$	$1.0470{\cdot}10^{-4}$	$8.6807{\cdot}10^{-3}$
11	1.3910	$6.0497{\cdot}10^{-4}$	$4.7930{\cdot}10^{-7}$	$4.0970{\cdot}10^{-4}$
12	1.3909	$8.0828{\cdot}10^{-6}$	$1.7092{\cdot}10^{-9}$	$5.3431{\cdot}10^{-6}$
13	1.3909	$1.3646{\cdot}10^{-9}$	$2.7215{\cdot}10^{-13}$	$3.9812{\cdot}10^{-10}$

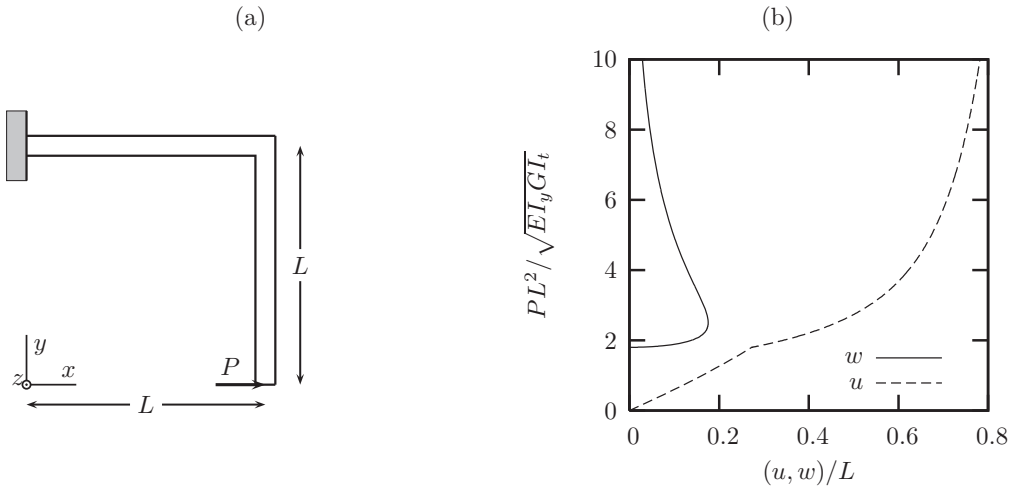

Figure 4. Right-angle frame: (a) geometry, (b) load-deflection curves.

Table IV. Right-angle frame, starting from the equilibrium point at P_*.

		iterations using constraint				
elements	P_*/ N	(38)	(39)	(40)	(41)	Wriggers-Simo
8	1	10	6	8	8	9
16	1	8	7	10	10	11
32	1	7	10	12	8	10
128	1	8	6	13	12	10
32	-1	9	7	9	7	9
128	-1	9	7	9	7	9
16	0	$10^\dagger$	div	$15^\dagger$	div	$16^\dagger$

† Converges to the negative critical load.

parameter γ. As noticed also by Wriggers and Simo, behaviour of the iteration is not sensitive to the value of the stabilization parameter.

For the extended system it seems to be a deceptively simple example. If the iteration is started from the initial undeformed configuration $P_* = 0$, the extended systems with constraints (38) and (40) converge to the negative critical load while with the constraints (39) and (41) do not converge. Also the stabilized extended system by Wriggers and Simo converges to the negative load.

5. CONCLUDING REMARKS

In this paper procedures for direct computation of critical equilibrium states for spatial beams and frames has been described. In the linearization of the extended system, second order derivatives of the residual vector with respect to the state variables are required, which are presented for the geometrically exact Reissner's beam model. The derivatives related to the rotation can also be utilized for geometrically exact shell models. The direct approach for the critical point computation is a reliable procedure only if the initial state is relatively close to the critical point due to the local convergence property of the Newton's iteration. The procedure is independent of element fomulations, if capable to handle large incremental displacements and rotations. Similar results as presented here have been obtained also for solid elements, see Ref. [43]. Further developments will be focused on enlarging the convergence domain to improve the robustness. A mixed strategy combining elements on linearized stability analysis, continuation method and the non-linear stability eigenvalue problem is under development.

APPENDIX

The tensors $\mathbf{C}_i, i = 1, 2, 3$ are defined by directional derivatives

$$\mathbf{C}_1(\mathbf{V}, \mathbf{\Psi}) \cdot \Delta\mathbf{\Psi} := \mathrm{D}_{\mathbf{\Psi}}(\mathbf{T} \cdot \mathbf{V}) \cdot \Delta\mathbf{\Psi}, \tag{67}$$

$$\mathbf{C}_2(\mathbf{V}, \mathbf{\Psi}) \cdot \Delta\mathbf{\Psi} := \mathrm{D}_{\mathbf{\Psi}}(\mathbf{T}^{\mathrm{T}} \cdot \mathbf{V}) \cdot \Delta\mathbf{\Psi}, \tag{68}$$

$$\mathbf{C}_3(\mathbf{V}, \mathbf{\Psi}', \mathbf{\Psi}) \cdot \Delta\mathbf{\Psi} := \mathrm{D}_{\mathbf{\Psi}}(\mathbf{C}_1^{\mathrm{T}}(\mathbf{\Psi}', \mathbf{\Psi}) \cdot \mathbf{V}) \cdot \Delta\mathbf{\Psi}, \quad \forall\, \mathbf{V} \in \mathsf{E}^3, \tag{69}$$

and have the following explicit expressions

$$\mathbf{C}_1(\mathbf{V}, \mathbf{\Psi}) = c_1 \mathbf{V} \otimes \mathbf{\Psi} - c_2(\tilde{\mathbf{\Psi}}\mathbf{V}) \otimes \mathbf{\Psi} + c_3(\mathbf{\Psi} \cdot \mathbf{V})\mathbf{\Psi} \otimes \mathbf{\Psi} - c_4\tilde{\mathbf{V}} + c_5\left((\mathbf{\Psi} \cdot \mathbf{V})\mathbf{I} + \mathbf{\Psi} \otimes \mathbf{V}\right), \tag{70}$$

$$\mathbf{C}_2(\mathbf{V}, \mathbf{\Psi}) = c_1 \mathbf{V} \otimes \mathbf{\Psi} + c_2(\tilde{\mathbf{\Psi}}\mathbf{V}) \otimes \mathbf{\Psi} + c_3\left(\mathbf{\Psi} \cdot \mathbf{V}\right)\mathbf{\Psi} \otimes \mathbf{\Psi} + c_4\tilde{\mathbf{V}} + c_5\left((\mathbf{\Psi} \cdot \mathbf{V})\mathbf{I} + \mathbf{\Psi} \otimes \mathbf{V}\right), \tag{71}$$

$$\begin{aligned}\mathbf{C}_3(\mathbf{V}, \mathbf{\Psi}', \mathbf{\Psi}) = {} & \Big(c_1\left(\mathbf{\Psi}' \cdot \mathbf{V}\right) + c_2(\mathbf{\Psi} \cdot \tilde{\mathbf{V}}\mathbf{\Psi}') + c_3(\mathbf{\Psi} \cdot \mathbf{\Psi}')(\mathbf{V} \cdot \mathbf{\Psi})\Big)\,\mathbf{I} + c_2(\mathbf{\Psi} \underset{\mathrm{S}}{\otimes} \tilde{\mathbf{V}}\mathbf{\Psi}') + \\ & + c_3(\mathbf{\Psi} \cdot \mathbf{\Psi}')\left(\mathbf{\Psi} \underset{\mathrm{S}}{\otimes} \mathbf{V}\right) + \frac{1}{\psi}\Big(c_1'\left(\mathbf{\Psi}' \cdot \mathbf{V}\right) + c_2'(\mathbf{\Psi} \cdot \tilde{\mathbf{V}}\mathbf{\Psi}') + c_3'(\mathbf{\Psi} \cdot \mathbf{\Psi}')(\mathbf{V} \cdot \mathbf{\Psi})\Big)\left(\mathbf{\Psi} \otimes \mathbf{\Psi}\right) + \\ & + c_3(\mathbf{V} \cdot \mathbf{\Psi})\left(\mathbf{\Psi} \underset{\mathrm{S}}{\otimes} \mathbf{\Psi}'\right) + c_5(\mathbf{\Psi}' \underset{\mathrm{S}}{\otimes} \mathbf{V}),\end{aligned} \tag{72}$$

where $\underset{\mathrm{S}}{\otimes}$ denotes the symmetric tensor product $(\mathbf{a} \underset{\mathrm{S}}{\otimes} \mathbf{b}) := (\mathbf{a} \otimes \mathbf{b}) + (\mathbf{b} \otimes \mathbf{a}), \quad \forall \mathbf{a}, \mathbf{b} \in \mathsf{E}^3$. The coefficients c_i and their derivatives are given by

$$c_1 := (\psi\cos\psi - \sin\psi)\psi^{-3}, \tag{73}$$

$$c_2 := (\psi\sin\psi + 2\cos\psi - 2)\psi^{-4}, \tag{74}$$

$$c_3 := (3\sin\psi - 2\psi - \psi\cos\psi)\psi^{-5}, \tag{75}$$

$$c_4 := (\cos\psi - 1)\psi^{-2}, \tag{76}$$

$$c_5 := (\psi - \sin\psi)\psi^{-3}, \tag{77}$$

$$c_1' = (3\sin\psi - \psi^2\sin\psi - 3\psi\cos\psi)\psi^{-4}, \tag{78}$$

$$c_2' = (\psi^2\cos\psi - 5\psi\sin\psi - 8\cos\psi + 8)\psi^{-5}, \tag{79}$$

$$c_3' = (7\psi\cos\psi + 8\psi + \psi^2\sin\psi - 15\sin\psi)\psi^{-6}, \tag{80}$$

$$c_1'' = (-\psi^3\cos\psi + 5\psi^2\sin\psi + 12\psi\,\cos\psi - 12\sin\psi)\psi^{-5}, \tag{81}$$

$$c_2'' = -(\psi^3\sin\psi + 8\psi^2\cos\psi - 28\psi\sin\psi - 40\cos\psi + 40)\psi^{-6}, \tag{82}$$

$$c_3'' = (\psi^3\cos\psi - 11\psi^2\sin\psi - 50\psi\cos\psi - 40\psi + 90\sin\psi)\psi^{-7}. \tag{83}$$

The limit processes for the tensors $\mathbf{C}_i$ give

$$\lim_{\mathbf{\Psi}\to\mathbf{0}} \mathbf{C}_1(\mathbf{V}, \mathbf{\Psi}) = \tfrac{1}{2}\tilde{\mathbf{V}}, \tag{84}$$

$$\lim_{\mathbf{\Psi}\to\mathbf{0}} \mathbf{C}_2(\mathbf{V}, \mathbf{\Psi}) = -\tfrac{1}{2}\tilde{\mathbf{V}}, \tag{85}$$

$$\lim_{\mathbf{\Psi}\to\mathbf{0}} \mathbf{C}_3(\mathbf{V}, \mathbf{\Psi}', \mathbf{\Psi}) = -\tfrac{1}{3}(\mathbf{\Psi}' \cdot \mathbf{V})\mathbf{I} + \tfrac{1}{6}(\mathbf{\Psi}' \underset{\mathrm{S}}{\otimes} \mathbf{V}) \tag{86}$$

The time derivative of the transformation $\mathbf{T}$ is

$$\dot{\mathbf{T}}(\dot{\mathbf{\Psi}}, \mathbf{\Psi}) = c_1(\mathbf{\Psi} \cdot \dot{\mathbf{\Psi}})\mathbf{I} - c_2(\mathbf{\Psi} \cdot \dot{\mathbf{\Psi}})\tilde{\mathbf{\Psi}} + c_3(\mathbf{\Psi} \cdot \dot{\mathbf{\Psi}})\mathbf{\Psi} \otimes \mathbf{\Psi} + c_4\dot{\tilde{\mathbf{\Psi}}} + c_5(\dot{\mathbf{\Psi}} \otimes \mathbf{\Psi} + \mathbf{\Psi} \otimes \dot{\mathbf{\Psi}}), \tag{87}$$

where the coefficients are given in (73). The limit value of the tensor $\dot{\mathbf{T}}$ is

$$\lim_{\boldsymbol{\Psi}\to\mathbf{0}} \dot{\mathbf{T}}(\dot{\boldsymbol{\Psi}},\boldsymbol{\Psi}) = -\tfrac{1}{2}\dot{\tilde{\boldsymbol{\Psi}}}. \tag{88}$$

The tensors $\mathbf{C}_i, i = 7,\dots,10$ are defined by directional derivatives

$$\mathbf{C}_7(\mathbf{W},\mathbf{V},\boldsymbol{\Psi})\cdot\Delta\boldsymbol{\Psi} := \mathrm{D}_{\boldsymbol{\Psi}}\left(\mathbf{C}_2(\mathbf{V},\boldsymbol{\Psi})\cdot\mathbf{W}\right)\cdot\Delta\boldsymbol{\Psi}, \tag{89}$$

$$\mathbf{C}_8(\mathbf{W},\mathbf{V},\boldsymbol{\Psi})\cdot\Delta\boldsymbol{\Psi} := \mathrm{D}_{\boldsymbol{\Psi}}\left(\mathbf{C}_1(\mathbf{V},\boldsymbol{\Psi})\cdot\mathbf{W}\right)\cdot\Delta\boldsymbol{\Psi}, \tag{90}$$

$$\mathbf{C}_9(\mathbf{X},\mathbf{W},\boldsymbol{\Psi})\cdot\Delta\mathbf{V} := \mathrm{D}_{\mathbf{V}}\left(\mathbf{C}_3(\mathbf{W},\mathbf{V},\boldsymbol{\Psi})\cdot\mathbf{X}\right)\cdot\Delta\mathbf{V}, \tag{91}$$

$$\mathbf{C}_{10}(\mathbf{X},\mathbf{W},\mathbf{V},\boldsymbol{\Psi})\cdot\Delta\boldsymbol{\Psi} := \mathrm{D}_{\boldsymbol{\Psi}}\left(\mathbf{C}_3(\mathbf{W},\mathbf{V},\boldsymbol{\Psi})\cdot\mathbf{X}\right)\cdot\Delta\boldsymbol{\Psi}, \tag{92}$$

$$\mathrm{D}_{\mathbf{W}}\left(\mathbf{C}_3(\mathbf{W},\mathbf{V},\boldsymbol{\Psi})\cdot\mathbf{X}\right) = \dot{\mathbf{C}}_1^{\mathrm{T}}(\mathbf{X},\mathbf{V},\boldsymbol{\Psi}), \tag{93}$$

$$\mathrm{D}_{\mathbf{V}}\left(\mathbf{C}_1(\mathbf{V},\boldsymbol{\Psi})\cdot\mathbf{W}\right) = \dot{\mathbf{T}}(\mathbf{W},\boldsymbol{\Psi}), \tag{94}$$

$$\mathrm{D}_{\mathbf{V}}\left(\mathbf{C}_2(\mathbf{V},\boldsymbol{\Psi})\cdot\mathbf{W}\right) = \dot{\mathbf{T}}^{\mathrm{T}}(\mathbf{W},\boldsymbol{\Psi}), \quad \forall\,\mathbf{V},\mathbf{W},\mathbf{X}\in\mathsf{E}^3, \tag{95}$$

and have the following explicit expressions

$$\begin{aligned}\mathbf{C}_7(\mathbf{W},\mathbf{V},\boldsymbol{\Psi}) &= c_1\mathbf{V}\otimes\mathbf{W} - c_2(\boldsymbol{\Psi}\cdot\mathbf{W})\tilde{\mathbf{V}} + c_2\tilde{\boldsymbol{\Psi}}\mathbf{V}\otimes\mathbf{W} + c_3(\boldsymbol{\Psi}\cdot\mathbf{W})\boldsymbol{\Psi}\otimes\mathbf{V} + c_3(\boldsymbol{\Psi}\cdot\mathbf{V})\boldsymbol{\Psi}\otimes\mathbf{W} + \\ &+ \left(c_3(\boldsymbol{\Psi}\cdot\mathbf{W})(\boldsymbol{\Psi}\cdot\mathbf{V}) + c_5(\mathbf{W}\cdot\mathbf{V})\right)\mathbf{I} + c_5\mathbf{W}\otimes\mathbf{V} + \frac{c_1'}{\psi}(\boldsymbol{\Psi}\cdot\mathbf{W})\mathbf{V}\otimes\boldsymbol{\Psi} + \frac{c_2'}{\psi}(\boldsymbol{\Psi}\cdot\mathbf{W})\tilde{\boldsymbol{\Psi}}\mathbf{V}\otimes\boldsymbol{\Psi} + \\ &+ \left(\frac{c_3'}{\psi}(\boldsymbol{\Psi}\cdot\mathbf{V})(\boldsymbol{\Psi}\cdot\mathbf{W}) + c_3(\mathbf{W}\cdot\mathbf{V})\right)\boldsymbol{\Psi}\otimes\boldsymbol{\Psi} - c_2\tilde{\mathbf{V}}\mathbf{W}\otimes\boldsymbol{\Psi} + c_3(\boldsymbol{\Psi}\cdot\mathbf{V})\mathbf{W}\otimes\boldsymbol{\Psi}\end{aligned} \tag{96}$$

$$\begin{aligned}\mathbf{C}_8(\mathbf{W},\mathbf{V},\boldsymbol{\Psi}) &= c_1\mathbf{V}\otimes\mathbf{W} + c_2(\boldsymbol{\Psi}\cdot\mathbf{W})\tilde{\mathbf{V}} - c_2\tilde{\boldsymbol{\Psi}}\mathbf{V}\otimes\mathbf{W} + c_3(\boldsymbol{\Psi}\cdot\mathbf{W})\boldsymbol{\Psi}\otimes\mathbf{V} + c_3(\boldsymbol{\Psi}\cdot\mathbf{V})\boldsymbol{\Psi}\otimes\mathbf{W} + \\ &+ \left(c_3(\boldsymbol{\Psi}\cdot\mathbf{W})(\boldsymbol{\Psi}\cdot\mathbf{V}) + c_5(\mathbf{W}\cdot\mathbf{V})\right)\mathbf{I} + c_5\mathbf{W}\otimes\mathbf{V} + \frac{c_1'}{\psi}(\boldsymbol{\Psi}\cdot\mathbf{W})\mathbf{V}\otimes\boldsymbol{\Psi} - \frac{c_2'}{\psi}(\boldsymbol{\Psi}\cdot\mathbf{W})\tilde{\boldsymbol{\Psi}}\mathbf{V}\otimes\boldsymbol{\Psi} + \\ &+ \left(\frac{c_3'}{\psi}(\boldsymbol{\Psi}\cdot\mathbf{V})(\boldsymbol{\Psi}\cdot\mathbf{W}) + c_3(\mathbf{W}\cdot\mathbf{V})\right)\boldsymbol{\Psi}\otimes\boldsymbol{\Psi} + c_2\tilde{\mathbf{V}}\mathbf{W}\otimes\boldsymbol{\Psi} + c_3(\boldsymbol{\Psi}\cdot\mathbf{V})\mathbf{W}\otimes\boldsymbol{\Psi}\end{aligned} \tag{97}$$

$$\mathbf{C}_9(\mathbf{W},\mathbf{V},\boldsymbol{\Psi}) = \mathbf{C}_7^{\mathrm{T}}(\mathbf{W},\mathbf{V},\boldsymbol{\Psi}) \tag{98}$$

$$\begin{aligned}\mathbf{C}_{10}(\mathbf{X},\mathbf{V},\boldsymbol{\Psi}',\boldsymbol{\Psi}) &= \left(c_2(\tilde{\mathbf{V}}\boldsymbol{\Psi}'\cdot\mathbf{X}) + c_3(\boldsymbol{\Psi}\cdot\boldsymbol{\Psi}')(\mathbf{V}\cdot\mathbf{X}) + c_3(\mathbf{V}\cdot\boldsymbol{\Psi})(\boldsymbol{\Psi}'\cdot\mathbf{V})\right)\mathbf{I} + \\ &+ \frac{1}{\psi^2}\left(c_1''(\boldsymbol{\Psi}'\cdot\,\mathbf{V}) + c_2''(\boldsymbol{\Psi}\cdot\,\tilde{\mathbf{V}}\boldsymbol{\Psi}') + c_3''(\boldsymbol{\Psi}\,\cdot\,\boldsymbol{\Psi}')(\mathbf{V}\,\cdot\,\boldsymbol{\Psi})\right)(\boldsymbol{\Psi}\cdot\mathbf{X})\boldsymbol{\Psi}\otimes\boldsymbol{\Psi} + \\ &+ \frac{1}{\psi}\left(c_3'(\mathbf{V}\cdot\boldsymbol{\Psi})(\boldsymbol{\Psi}'\cdot\mathbf{X}) + c_3'(\boldsymbol{\Psi}'\cdot\boldsymbol{\Psi})(\mathbf{V}\cdot\mathbf{X}) + c_2'(\tilde{\mathbf{V}}\boldsymbol{\Psi}'\cdot\mathbf{X})\right)\boldsymbol{\Psi}\otimes\boldsymbol{\Psi} + \\ &+ \frac{1}{\psi}\left(c_1'(\boldsymbol{\Psi}'\cdot\mathbf{V}) + c_2'(\boldsymbol{\Psi}\cdot\tilde{\mathbf{V}}\boldsymbol{\Psi}') + c_3'(\boldsymbol{\Psi}\cdot\boldsymbol{\Psi}')(\mathbf{V}\cdot\boldsymbol{\Psi})\right)(\boldsymbol{\Psi}\cdot\mathbf{X})(\mathbf{I} - \frac{1}{\psi^2}\boldsymbol{\Psi}\otimes\boldsymbol{\Psi}) + c_2\mathbf{X}\underset{\mathrm{S}}{\otimes}\tilde{\mathbf{V}}\boldsymbol{\Psi}' + \\ &+ \left(c_3(\mathbf{V}\cdot\mathbf{X}) + \frac{c_3'}{\psi}(\boldsymbol{\Psi}\cdot\mathbf{X})(\mathbf{V}\cdot\boldsymbol{\Psi})\right)\boldsymbol{\Psi}\underset{\mathrm{S}}{\otimes}\boldsymbol{\Psi}' + c_3(\mathbf{V}\cdot\boldsymbol{\Psi})\mathbf{X}\underset{\mathrm{S}}{\otimes}\boldsymbol{\Psi}' + c_3(\boldsymbol{\Psi}\cdot\boldsymbol{\Psi}')\mathbf{X}\underset{\mathrm{S}}{\otimes}\mathbf{V} + c_3(\mathbf{X}\cdot\boldsymbol{\Psi})\mathbf{V}\underset{\mathrm{S}}{\otimes}\boldsymbol{\Psi} + \\ &+ \frac{1}{\psi}\left(c_1'(\boldsymbol{\Psi}'\cdot\mathbf{V}) + c_2'(\boldsymbol{\Psi}\cdot\tilde{\mathbf{V}}\boldsymbol{\Psi}') + c_3'(\boldsymbol{\Psi}\cdot\boldsymbol{\Psi}')(\mathbf{V}\cdot\boldsymbol{\Psi})\right)\boldsymbol{\Psi}\underset{\mathrm{S}}{\otimes}\mathbf{X} + \\ &+ \left(c_3(\boldsymbol{\Psi}'\cdot\mathbf{X}) + \frac{c_3'}{\psi}(\boldsymbol{\Psi}\cdot\mathbf{X})(\boldsymbol{\Psi}\cdot\boldsymbol{\Psi}')\right)\boldsymbol{\Psi}\underset{\mathrm{S}}{\otimes}\mathbf{V}\frac{1}{\psi}c_2'(\mathbf{X}\cdot\boldsymbol{\Psi})\boldsymbol{\Psi}\underset{\mathrm{S}}{\otimes}\tilde{\mathbf{V}}\boldsymbol{\Psi}'\end{aligned} \tag{99}$$

$$\dot{\mathbf{C}}_1(\mathbf{W},\mathbf{V},\boldsymbol{\Psi}) = \mathbf{C}_8(\mathbf{W},\mathbf{V},\boldsymbol{\Psi}) \tag{100}$$

The limit processes for the tensors $\mathbf{C}_i, i = 7, 8, 10$ give

$$\lim_{\boldsymbol{\Psi}\to\mathbf{0}} \mathbf{C}_7(\mathbf{W},\mathbf{V},\boldsymbol{\Psi}) = -\tfrac{1}{3}\mathbf{V}\otimes\mathbf{W} + \tfrac{1}{6}\left(\mathbf{W}\otimes\mathbf{V} + (\mathbf{W}\cdot\mathbf{V})\mathbf{I}\right) \tag{101}$$

$$\lim_{\boldsymbol{\Psi}\to\mathbf{0}} \mathbf{C}_8(\mathbf{W},\mathbf{V},\boldsymbol{\Psi}) = -\tfrac{1}{3}\mathbf{V}\otimes\mathbf{W} + \tfrac{1}{6}\left(\mathbf{W}\otimes\mathbf{V} + (\mathbf{W}\cdot\mathbf{V})\mathbf{I}\right), \tag{102}$$

$$\lim_{\boldsymbol{\Psi}\to\mathbf{0}} \mathbf{C}_{10}(\mathbf{X},\mathbf{V},\boldsymbol{\Psi}',\boldsymbol{\Psi}) = -\tfrac{1}{12}(\tilde{\mathbf{V}}\boldsymbol{\Psi}'\cdot\mathbf{X})\mathbf{I} - \tfrac{1}{12}\mathbf{X}\underset{\mathrm{S}}{\otimes}\tilde{\mathbf{V}}\boldsymbol{\Psi}' \tag{103}$$

REFERENCES

1. Attard M. Lateral buckling analysis of beams by the FEM. *Computers and Structures* 1986; .
2. Chang SC, Chen J. Effectiveness of linear bifurcation analysis for predicting the nonlinear stability limits of structures. *International Journal for Numerical Methods in Engineering* 1986; **23**(5):831–846.
3. Erp G. Advanced buckling analyses of beams with arbitrary cross sections. PhD Thesis, Eindhoven University of Technology 1989.
4. Huitfeldt J. Nonlinear eigenvalue problems - prediction of bifurcation points and branch switching. *Technical Report 17*, Department of Computer Sciences, Chalmers University of technology 1991.
5. Huitfeldt J, Ruhe A. A new algorithm for numerical path following applied to an example from hydrodynamic flow. *SIAM Journal on Scientific and Statistical Computing* 1990; **11**:1181–1192.
6. Riks E. The incremental solution of some basic problems in elastic stability. *Technical Report NLR TR 74005 U*, National Aerospace Laboratory, The Netherlands 1974.
7. Riks E. An incremental approach to the solution of snapping and buckling problems. *International Journal of Solids and Structures* 1979; **15**:529–551.
8. Bergan P, Horrigmoe G, Kråkeland B. Solution techniques for nonlinear finite element problems. *International Journal for Numerical Methods in Engineering* 1978; **12**:1677–1696.
9. Wagner W, Wriggers P. A simple method for the calculation of postcritical branches. *Engineering Computation* 1988; **5**:103–109.
10. Abbot J. An efficient algorithm for the determination of certain bifurcation points. *Journal Computational and Applied Mathematics* 1987; **4**:19–27.
11. Planinc I, Saje M. A quadratically convergent algorithm for the computation of stability points: The application of the determinant of the tangent stiffness matrix. *Computer Methods in Applied Mechanics and Engineering* 1999; **169**:89–105.
12. Battini JM, Pacoste C, Eriksson A. Improved minimal augmentation procedure for the direct computation of critical points. *Computer Methods in Applied Mechanics and Engineering* 2003; **192**(16-18):2169–2185.
13. Keener J, Keller H. Perturbed bifurcation theory. *Archive for Rational Mechanics and Analysis* 1973; **50**:159–175.
14. Seydel R. Numerical computation of branch points in nonlinear equations. *Numerische Mathematik* 1979; **33**:339–352.
15. Fink J, Rheinboldt W. The role of tangent mapping in analyzing bifurcation behaviour. *Zeitschrift für Angewandte Mathematik und Mechanik* 1984; **64**(9):407–412.
16. Wriggers P, Wagner W, Miehe C. A quadratically convergent procedure for the calculation of stability points in finite element analysis. *Computer Methods in Applied Mechanics and Engineering* 1988; **70**:329–347.
17. Wriggers P, Simo J. A general procedure for the direct computation of turning and bifurcation problems. *International Journal for Numerical Methods in Engineering* 1990; **30**:155–176.
18. Cardona A, Huespe A. Evaluation of simple bifurcation points and post-critical path in large finite rotation problems. *Computer Methods in Applied Mechanics and Engineering* 1999; **175**(1–2):137–156.
19. Ibrahimbegović A, Mikdad MA. Quadratically convergent direct calculation of critical points for 3d structures undergoing finite rotations. *Computer Methods in Applied Mechanics and Engineering* 2000; **189**:107–120.
20. Wu B. Numerical non-linear analysis of secondary buckling in stability problems. *Computer Methods in Applied Mechanics and Engineering* 1995; **120**(1–2):183–193.
21. Keener J. Perturbed bifurcation theory at multiple eigenvalues. *Archive for Rational Mechanics and Analysis* 1974; **56**:348–366.
22. Simo J. A finite strain beam formulation. the three dimensional dynamic problem, Part I. *Computer Methods in Applied Mechanics and Engineering* 1985; **49**:55–70.

23. Simo J, Vu-Quoc L. A three dimensional finite strain rod model, Part II: Computational aspect. *Computer Methods in Applied Mechanics and Engineering* 1986; **58**:79–115.
24. Cardona A, Geradin M. A beam finite element non-linear theory with finite rotations. *International Journal for Numerical Methods in Engineering* 1988; **26**(11):2403–2438.
25. Ibrahimbegović A. On finite element implementation of geometrically nonlinear reissners's beam theory: three-dimensional curved beam elements. *Computer Methods in Applied Mechanics and Engineering* 1995; **122**(1–2):11–26.
26. Jelenić G, Saje M. A kinematically exact space finite strain beam model – finite element formulation by generalized virtual work principle. *Computer Methods in Applied Mechanics and Engineering* 1995; **120**(1–2):131–161.
27. Jelenić G, Crisfield M. Geometrically exact 3d beam theory: implementation of a strain-invariant finite element for statics and dynamics. *Computer Methods in Applied Mechanics and Engineering* 1999; **171**(1–2):141–171.
28. Betsch P, Steinmann P. Frame indifferent beam finite element based upon the geometrically exact beam theory. *International Journal for Numerical Methods in Engineering* 2002; **54**:1775–1788.
29. Romero I, Armero F. An objective finite element approximation of the kinematics of geometrically exact rods and its use in the formulation of an energy-momentum conserving scheme in dynamics. *International Journal for Numerical Methods in Engineering* 2002; **54**(12):1683–1716.
30. Mäkinen J. Total Lagrangian Reissner's geometrically exact beam element without singularities. *International Journal for Numerical Methods in Engineering* 2007; **70**:1009–1048.
31. Auricchio F, Carotenuto P, Reali A. On the geometrically exact beam model: A consistent, effective and simple derivation from three-dimensional finite elasticity. *International Journal of Solids and Structures* 2008; **45**(17):4766–4781.
32. Mäkinen J. Rotation manifold SO(3) and its tangential vectors. *Computational Mechanics* 2008; **42**:907–919.
33. Werner B, Spence A. The computation of symmetry-breaking bifurcation points. *SIAM Journal on Numerical Analysis* 1984; **21**:388–399.
34. Eriksson A. Derivatives of tangential stiffness matrices for equilibrium path descriptions. *International Journal for Numerical Methods in Engineering* 1991; **32**:1093–1113.
35. Eriksson A. Fold lines for sensitivity analyses in structural instability. *Computer Methods in Applied Mechanics and Engineering* 1994; **114**:77–101.
36. Lopez S. Detection of bifurcation points along a curve traced by a continuation method. *International Journal for Numerical Methods in Engineering* 2002; **53**:983–1004.
37. Lopez S. Post-critical analysis of structures with a nonlinear pre-buckling state in the presence of imperfections. *Computer Methods in Applied Mechanics and Engineering* 2002; **191**:4421–4440.
38. Magnusson A, Svensson I. Numerical treatment of complete load-deflection curves. *International Journal for Numerical Methods in Engineering* 1998; **41**:955–971.
39. Ortega J, Rheinboldt W. *Iterative Solution of Nonlinear Equations in Several Variables*. Academic Press, 1970.
40. Kelley C. *Iterative Methods for Linear and Nonlinear Equations*. SIAM, 1995.
41. Govaerts W. *Numerical methods for bifurcations of dynamic equilibria*. SIAM, 2000.
42. Vannucci P, Cochelin B, Damil N, Potier-Ferry M. An asymptotic-numerical method to compute bifurcating branches. *International Journal for Numerical Methods in Engineering* 1998; **41**(8):1365–1389.
43. Mäkinen J, Kouhia R, Fedoroff A, Marjamäki H. Implementation of a direct procedure for critical point computations. *Proceedings of the Tenth International Conference on Engineering Computational technology*, Topping B, Adam J, Pallarés F, Bru R, Romero M (eds.), Civil-Comp Press: Strirlingshire, United Kingdom, 2010. URL `http://dx.doi.org/10.4203/ccp.93.152`, paper 152.
44. Chu KH, Rampetsreiter R. Large deflection buckling of space frames. *Journal of Structural Division, ASCE* 1972; **98**:2701–2711.